Fabrication of $Ni_{0.5}Mg_{0.5}Fe_2O_4$/Reduced Graphene Oxide Based Electrochemical Sensor for the Detection of Lead

By

Muhammad Umair Idrees

School of Chemical and Materials Engineering (SCME)

National University of Sciences and Technology (NUST)

2017

Fabrication of $Ni_{0.5}Mg_{0.5}Fe_2O_4$/Reduced Graphene Oxide Based Electrochemical Sensor for the Detection of Lead

Name: Muhammad Umair Idrees

Reg. No: NUST201463900MSCME67914F

This thesis is submitted as a partial fulfillment of the requirements for the degree of

MS Nanoscience and Engineering

Supervisor Name: Dr. Zakir Hussain

School of Chemical and Materials Engineering (SCME)

National University of Sciences and Technology (NUST), H-12

Islamabad, Pakistan

February 2017

THESIS ACCEPTANCE CERTIFICATE

Certified that final copy of MS/MPhil thesis written by **Mr. Muhammad Umair Idrees** (Registration No. NUST201463900MSCME67914F), of School of Chemical and Materials Engineering (SCME) has been vetted by undersigned, found complete in all respects as per NUST Statues/Regulations, is free of plagiarism, errors, mistakes and is accepted as partial fulfillment for award of MS/MPhil degree. It is further certified that necessary amendments as pointed out by GEC members of the scholar have also been incorporated in the said thesis.

Signature: _____

Name of Supervisor: **Dr. Zakir Hussain**

Date: _____

Signature (HOD): _____

Date: _____

Signature (Dean/Principle): _____

Date: _____

Dedicated

To

My family and friends

for their endless love support and encouragement

ACKNOWLEDGEMENTS

All praises are to ALMIGHTY ALLAH, the merciful and beneficent, who bestowed the mankind with knowledge and wisdom and made him able to disclose the secrets of the universe. Thanks to the Holy Prophet Muhammad (Peace be upon him) and Al-e-Muhammad (Peace be upon him) who directed humanity to the true path of life (Islam).

The real spirit of achieving a goal is through the way of excellence and discipline. I would have never succeeded in completing my task without the cooperation, encouragement and help provided to me by various personalities.

With deep sense of gratitude I express my sincere thanks to my esteemed and worthy supervisor Dr. Zakir Hussain, for his valuable guidance in carrying out this work under his effective supervision, encouragement, enlightens and cooperation.

Special thanks to my GEC members Dr. Iftikhar Hussain Gul and Dr. Ahmad Nawaz khan for their timely help, cooperation and useful discussions. I am extremely thankful to all my teachers during my whole course of study for delivering their knowledge.

I am also grateful to staff of School of Chemical and Materials Engineering NUST for their extreme co-operation.

I am thankful to my friends specially Muzamil Ahmad Khan who helped me a lot, throughout my research work.

I shall be failing in my duties if I do not express my deep sense of gratitude towards my father who has been a constant source of inspiration for me throughout this work. Specially regards to my parents and friends for providing me every opportunity and support throughout my educational life.

Regards,
Muhammad Umair Idrees

Abstract:

Lead (Pb) is considered as one of the main toxic heavy metal that causes environmental contamination and certain severe problems to the human health. Therefore, trace level detection of lead in the environment is very much required. In this work, a highly sensitive sensor based on interdigitated electrode modified by sensing materials like $Ni_{0.5}Mg_{0.5}Fe_2O_4$ ferrites, graphene oxide and $Ni_{0.5}Mg_{0.5}Fe_2O_4$/rGO nanocomposite have been successfully fabricated for the detection of Pb. Scanning electron microscopy and X-ray diffraction characterization techniques have been performed for the morphological and structural studies of the sensing materials. SEM results show that the average particle size to be 20nm with no agglomeration and XRD results justify the formation of required sensing materials as all the relevant peaks are present. Linear sweep voltammetry, cyclic voltammetry and electrochemical impedance spectroscopy techniques have been used to observe the electrochemical response of fabricated sensor towards Pb^{2+} ions. Results reveal that IDEs modified by $Ni_{0.5}Mg_{0.5}Fe_2O_4$ ferrites show very low response towards Pb^{2+} ions while graphene oxide and $Ni_{0.5}Mg_{0.5}Fe_2O_4$/rGO nanocomposite modified IDEs show higher response when exposed to Pb^{2+} ions. Among the three sensing materials used, $Ni_{0.5}Mg_{0.5}Fe_2O_4$/rGO nanocomposite modified IDEs has higher sensitivity. The sensitivity achieved by using $Ni_{0.5}Mg_{0.5}Fe_2O_4$/rGO nanocomposite as a sensing element is 0.000389 μA ppb^{-1} and limit of detection (LOD) obtained is 7.06 ppb, which is much below the threshold limit (10ppb) set by the world health organization (WHO).

Table of Contents

List of Figures

List of Tables:

Chapter 1
Introduction

1.1 Heavy metals

Heavy metals are known due to their high electronegativity and are regarded as low density chemical components [1, 2]. These metals have a density higher than 5g cm^{-3} and atomic number higher than 20. Heavy metals are also well known due to their high toxicity which harms the environment and have a bad impact on human health. Few of them are arsenic (As), Lead (Pb), mercury (Hg), chromium (Cr), copper (Cu), Iron (Fe), cadmium (Cd). Some heavy metals such as iron (Fe), zinc (Zn) etc., are required in lower concentrations by living organisms for their better health, while exceeding the trace amounts can cause serious problems to health. Several heavy metals like arsenic (Ar), mercury (Hg) etc., are highly toxic and hazardous to health even at very lower concentrations [1, 3-5].

Many different sources of heavy metals are present in the environment. The main sources which lead to the excretion of these metals are given below (Table 1).

Source	As	Cd	Cr	Cu	Pb	Hg	Ni	Zn
Mining and ore processing	✓	✓	×	✓	×	✓	×	✓
Metallurgy	✓	✓	✓	✓	✓	✓	✓	✓
Chemical industry	✓	✓	✓	✓	✓	✓	×	✓
Alloys industry	×	×	×	×	✓	×	×	×
Paint industry	×	✓	✓	×	✓	×	×	✓
Glass industry	✓	×	×	×	✓	✓	×	×
Pulp and paper mills	×	×	✓	✓	✓	✓	✓	×
Leather tanning	✓	×	✓	×	×	✓	×	✓
Textile dyeing and printing	✓	✓	×	✓	✓	✓	✓	✓
Chemical fertilizer industry	✓	✓	✓	✓	✓	✓	✓	✓
Petroleum refining	✓	✓	✓	✓	✓	✓	×	✓
Coal burning	✓	✓	✓	✓	✓	✓	✓	×

Table 1 Several heavy metals and their source [2]

Heavy metals are largely disseminated in the environment through the above mentioned sources and are conveyed by rain into soil, sea water and surface waters.

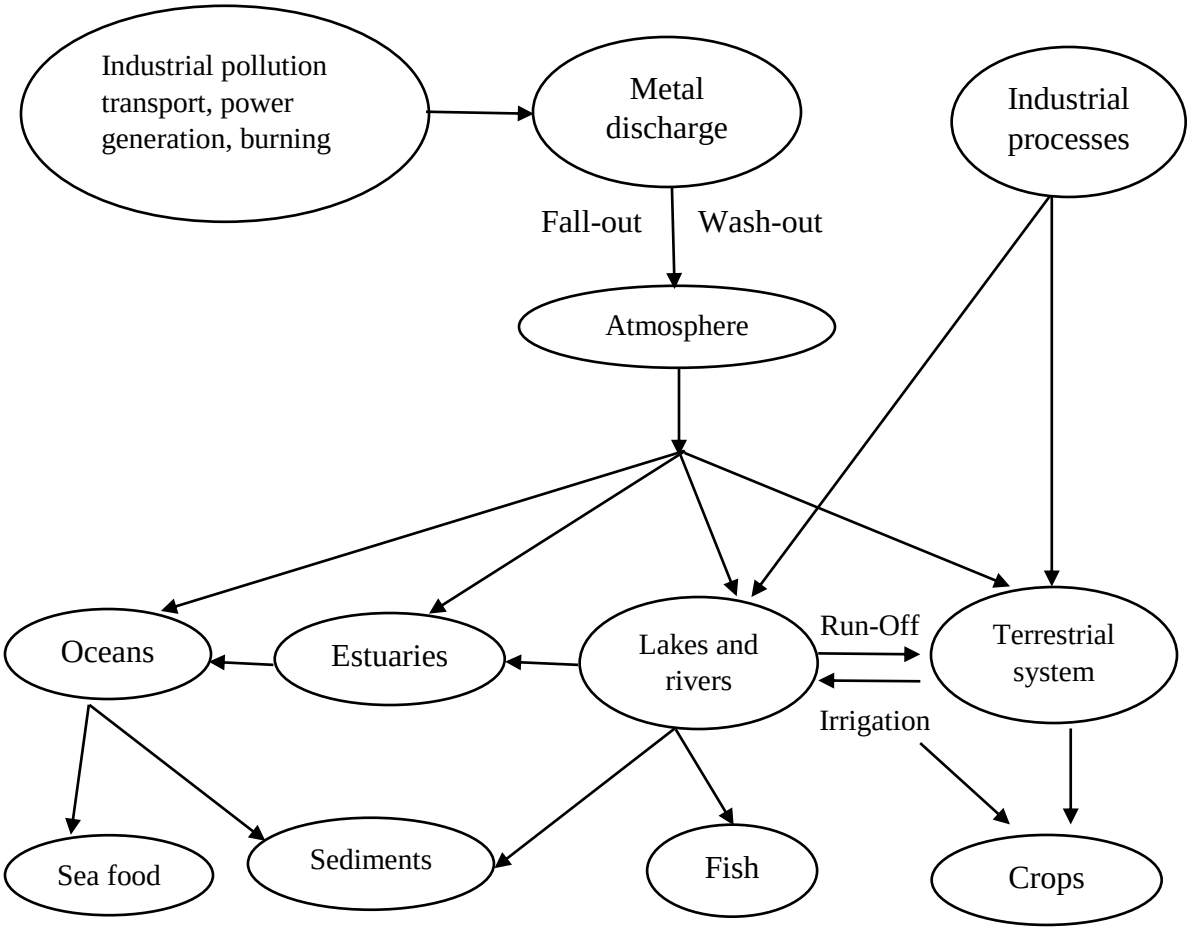

Figure 1.1 Distribution of metals in environment [2]

Human activities play major role in the contribution of heavy metals to the environment that include mining, burning, industrial waste etc. These activities by humans not only disseminate heavy metals into the land environment but also disturb the undersea and earthbound species. If consumed or inhaled by human beings, these heavy metals cause several diseases and affect kidneys, bones and nervous system [6].

Due to rapid industrialization, an increased release of heavy metals in waste water occurs that have an adverse effect on its surroundings. Among various heavy metals, chromium (Cr VI) is a contaminant which can be easily discovered because it is highly toxic and have a mobility higher than rest of the heavy metals. The amount of the

chromium in drinking water should not be more than 10ppb as prescribed by the World Health Organization (WHO). Drinking water contaminated with arsenic is an issue around the world as prolonged intake of arsenic causes cancer because of its carcinogenic nature. Pakistan and other countries like Bangladesh, New Zealand, and Taiwan have an arsenic-contaminated groundwater as a main source of drinking water. In Lahore Pakistan, water used for irrigation exceeds the allowable limit of Chromium. Both (organic and inorganic) forms of arsenic can exist. Generally inorganic As compounds are more toxic than organic As compounds, and As(III) is much more mobile and more toxic than As(V) [7-10].

Lead (Pb^{2+}) is a common and highly toxic pollutant in the environment whose prolonged exposure even at very low concentrations causes harmful effects to human health such as renal malfunctioning, brain damage and kidney failure [11]. The intake of lead in higher concentrations causes damage to the brain and physical unfitness in children while in adults it can damage the nervous system [12, 13].

Similarly, mercury (Hg) is another toxic heavy metal that has has worst effects on living organisms causing failure of kidney, disorders in the nervous system and even leads to death [14, 15]. The intake of low doses of mercury is very dangerous to health because it assembles in the body and causes very serious problems to health [16]. WHO allows a maximum limit of mercury in drinking water of about 2µg L^{-1}. The limit of mercury in human body can be investigated from blood samples, urine or hair samples. The blood absorbs certain amount of mercury while rest is eliminated with urine. Cysteine is an amino acid that readily binds with the mercury and is absorbed by the hairs which can be easily analyzed [15].

For the detection and remediation of heavy metals, a wide range of techniques have been used that include cyanides [7], electrochemical precipitation [17], adsorption [18], electrochemical sensors [19], colorimetric sensors [20] flotation and ultrasonic-assisted extraction [21]. Cyanide technique is not the promising one because during chlorination intermediates are formed which are highly toxic. These intermediates react with chlorine and cause further contamination to the environment. Precipitation through electrochemical technique is relevant and low cost, but this technique is not suitable

because it requires additional treatment for the sludge resulting in large amount through precipitation. Also, reprocessing and distinguishing these materials proves to be challenging as the particle size approaches to nanoscale. Accordingly, looking at the above challenges, adsorption has been found as the most executable and favorable technique because it is low in cost and has greater efficiency for the remediation of these hazardous metals through environment even at nanoscale. This technique can also be effectively used even at lower concentrations. Many adsorbents are used for the purification of water such as activated carbon, iron minerals, graphene, graphene oxide and many different composites. Although, activated carbon is mostly used for the purification of contaminated water but it lacks the ability to lower the concentrations of pollutants to the trace levels. Iron ores have been discerned as an effectual medium for the elimination of heavy metals such as arsinite, arsenate, chromium and lead from the environment mainly from the contaminated drinking water. Nanostructures of iron and its oxide have been established as much effective materials for the elimination of heavy metals [7, 17-20]. Several morphologies of nanoparticles like rods, tubes, wires and spheres have been used for the removal of contaminants from the polluted water. Magnetic nanospheres have the potential for the remediation of polluted water due to its high surface area and magnetic control [22]. One of the best method for detecting heavy metals is by using electrochemical sensor which is also mainly focused in these chapters. Electrochemical sensors are also able to sense heavy metals from polluted water. These sensors are highly sensitive and are precise in their detection.

1.2 Ferrite nanoparticles

Ferrites are the ferrimagnetic content that reveal significant spontaneous magnetization. They are also termed as oxides of iron containing another metal. According to their crystal structure these magnetic nanoparticles classify primarily into two categories.

1. Cubic/Spinel: These type of nanoparticles have the universal formula $M.Fe_2O_4$, where M is the metal ion such aSs Ni, Co, Zn, Mg, Fe or Mn. All metal ions have the valency of +2 [23].

2. Hexagonal: Barium and strontium ferrites are the important one in this. These ferrites are referred as magnetically hard [24].

1.3 Types of Magnetism

1. Diamagnetism
2. Paramagnetism
3. Ferromagnetism
4. Antiferromagnetism
5. Ferrimagnetism

1.3.1 Diamagnetism

In diamagnetic materials there is no net magnetic moment of an atom because the electrons are oriented in such a way that they cancel each other leaving behind zero or no net magnetic moment. This effect is found in all kinds of materials and considered as a weak effect [25].

1.3.2 Paramagnetism

In paramagnetic materials the magnetic moments are pointed arbitrarily and the overall magnetic moment is zero. Solids usually exhibits paramagnetic behavior, the atoms and ions that are referred to as permanent magnets.

In the absence of magnetic field, the magnetic moments are pointed arbitrarily and when the magnetic field is applied the magnetic moments points themselves in the direction of magnetic field and thus a magnetization is produced in the direction of applied field [26] (figure 1.2).

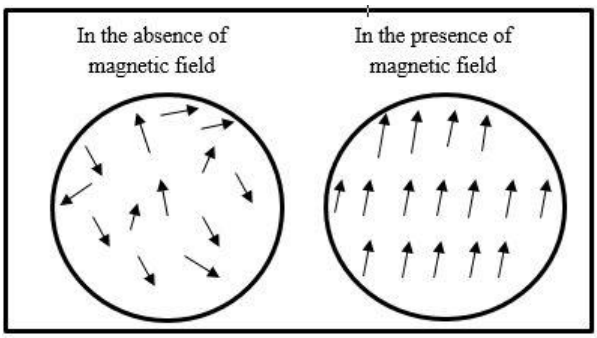

Figure 1.2 In the absence and presence of magnetic field

1.3.3 Ferromagnetism

Ferromagnetism is linked with the existence of enduring magnetic dipoles. Unlike Paramagnetism, the magnetic moments of adjoining atoms are lined up in a specific direction even when there is no magnetic field present. These adjoining atoms are aligned in a compact section called domains. When there is no magnetic field present the magnetization is referred as spontaneous magnetization. Ferromagnetic substances obtain elevated magnetization even when subjected to weak magnetic field. These ferromagnetic substances have the significant and positive susceptibility that changes with the change in the magnetic field, known as hysteresis loop [27] (Figure 1.3).

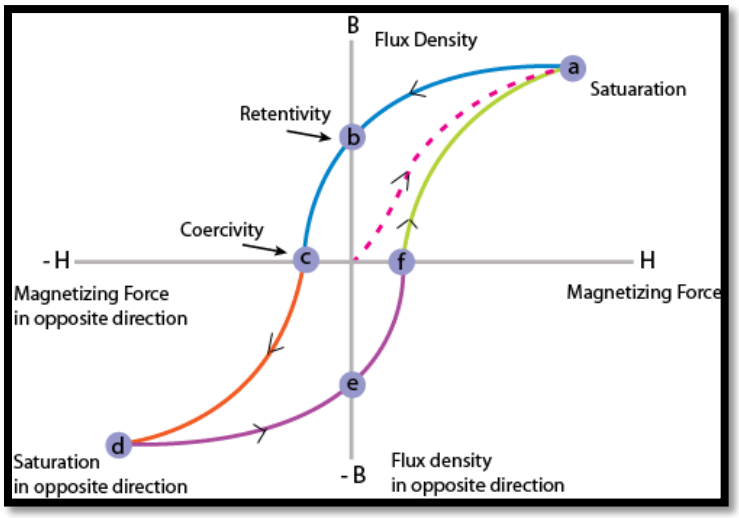

Figure 1.3 Hysteresis loop

Hysteresis loop is much essential for governing the materials quality and the selection of the material for a particular application.

1.3.4 Antiferromagnetism

In antiferromagnetism the spin moments of adjacent atoms ordered themselves in anti-parallel arrangement throughout the material (Figure 1.4). In the absence of an external magnetic field the magnetic moments of the neighboring atoms cancel each other resulting in the net zero magnetization. When the external magnetic field is applied, a slight magnetization is observed in the direction of the applied magnetic field. This magnetization varies with the temperature and increases with the increase in temperature.

The figure below shows the magnetic moments in the antiferromagnetism and also the difference between the antiferromagnetism and ferrimagnetism.

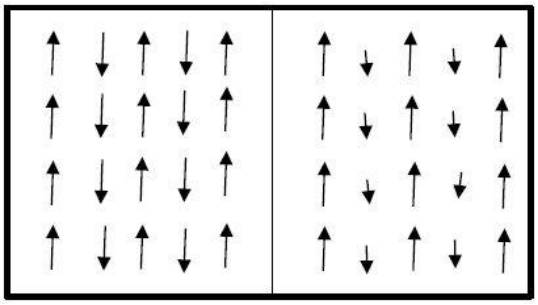

Figure 1.4 Difference between antiferromagnetism and ferrimagnetism

Manganese oxide is the first material in which antiferromagnetism was observed. At extremely low temperatures, the material shows no reaction when the external field is applied because the magnetic moments are arranged anti-parallel and are firmly asserted. When the temperature increases the atoms break the ordered arrangement and lined up in the direction of the applied magnetic field. When the magnetic moments are fully aligned, the magnetization tends to decrease with further increasing of the temperature [27].

1.3.5 Ferrimagnetism

In ferrimagnetism the adjacent magnetic moments are not equal in magnitude and the complete cancellation of moments does not occur as shown below (figure 1.5). Ferrimagnetism exhibits in the ferrites which are considerably different from the metal oxides. These magnetic ferrites fall mainly into two groups as described above.

1. Cubic
2. Hexagonal

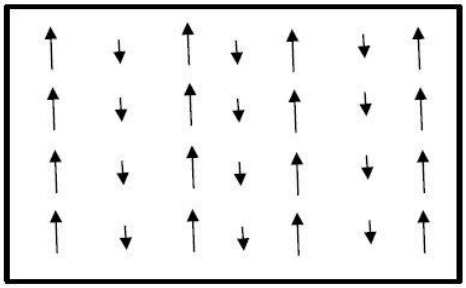

Figure 1.5 Magnetic moments are unequal and opposite in direction

Ferrites can play a vital role in the elimination of heavy metals contaminated water. Ferrites are considered to be an ideal adsorbents due to their high adsorption capability and they also exhibit excellent characteristics like superparamagnetism. S F Zhou reported the elimination of As(III) using mesoporous $MnFe_2O_4$ nanocrystal clusters. It was reported that As(III) was successfully removed from water using electrochemical detection by strong adsorption [28].

1.4 Graphene/Graphene Oxide

Graphene is a compelling material that has opened a new epoch of exploration because of its distinctive properties. Graphene is a one atom thick sheet of carbon and reveals especial chemical structure and magnificent electronic, thermal, optical and mechanical properties that makes it imperative for several engineering applications. Graphene and materials based on graphene are promising materials for manufacturing state-of-the-art sensors and bio-sensors at nano level [29]. These nano-sensors have high conductivity, large specific surface area, accomplish good accuracy, rapid action, high sensitivity, high selectivity, low limit of detection (LOD), and enduring stability. Due to the magnificent properties of grapheme, it can be used in many different applications such as composites, sensors, bio-medical applications and field effect transistors [29-31].

Graphene oxide is formed by the chemical modification of graphene either by oxidation or exfoliation. It also exhibits above mentioned applications because it contains the functional groups of reactive oxygen species on its surface. Many different applications can also be achieved by chemical functionalization of GO. GO can be chemically reduced using thermal, chemical or microwave treatment which reduces its oxygen content and is known as reduced graphene oxide (rGO) [32, 33].

1.4.1 Properties of Graphene/ Graphene Oxide

- **Electronic properties**

Graphene is a semiconductor having zero bandgap, exhibits ambipolar effect in electric field and charge carries can be tuned continual between electrons and holes. As an outcome of the structure of the graphene the 1st brillouin zone consists of two points K and K’ which are not equivalent and are known as Dirac points. The Dirac point is a point

where a conduction and valence band crosses each other. At this point the density of state is zero, resulting in low electrical conductivity. Doping is used for the improvement in electrical conductivity by changing its Fermi level. Experimental observations show the mobilities at room temperature up to 15000 $cm^2V^{-1}s^{-1}$. These mobilities which were monitored at room temperature are weakly dependent on the temperature, proposing that the extreme value of mobility can be realized at room temperature [34]. A elevated value of 200000 $cm^2V^{-1}s^{-1}$ can be achieved by reducing the impurity scattering [35]. Devices which are doped electrically or chemically, exhibits high mobilities showing the ballistic transport which means they can travel in sub-micron range [33].

- **Mechanical properties**

Graphene is the strongest material having 130GPa tensile strength and stiffness of about 1TPa. 0.142nm of C-C bond length is observed in graphene. It is also considered as one of the lightest material on earth and is examined as 1000 times lighter than 1 square meter of paper. A 1gram of graphene sheet is used to cover the whole football ground. Atomic force microscopy (AFM) measures the intrinsic breaking strength and shows the elastic properties of graphene. The mechanical properties can be further improved by chemical cross linking of separated platelets with polyallylamine [36].

- **Optical properties**

Graphene exhibits distinctive optical properties. This unique property makes a surprisingly high opacity in graphene which absorbs 2.3% of red light, which results from very low energy band in graphene. This low energy band is due to the interaction of conduction and valence band known as Dirac point. The graphene bandgap can be altered from 0-2.5eV on the application of voltage to the FET. Graphene/graphene oxide allows tuning of optical properties due to its unique electrochromic behavior. [33, 37].

1.5 Composites

Composites are the kind of materials that can be synthesized by the reinforcement of a matrix with a filler. Nanocomposites having remarkable properties can be synthesized using the reinforcement of nanocomposites and fibers with different materials like polymers, ceramic or metals [38].

1.5.1 Nanocomposites

Nanocomposites are those having one of the phase in the nanometer regime. These materials have high performance, show promising features with distinctive properties and have many different applications varying from packaging to bio-medical. There is a huge interest shown in the past few years with an annual growth rate of about 25%. As we move down to the nanoscale the properties of the material such as electrical conductivity, mechanical strength, insulating properties, elasticity changes abruptly. As the material approaches the nanometer scale there is an improvement in the interface interaction and this results in the enhancement of properties of the material [39]. There are many different types of nanocomposites some of them are listed as:

1.5.2 Polymer nanocomposites

Polymer nanocomposite consists of block copolymer and doped polymers. These polymers are doped with metals, ceramic and sometimes with semiconducting nanoparticles. Material properties such as electronic and thermo-mechanical improve by adding nanoparticles to the polymers. Some of the examples are given below:

- By doping the polymer with the nanoclay, barrier properties shows the enhancement, and also increase in the mechanical properties [40].
- Insulating properties showed up by doping the epoxies with nanoparticles. These type of insulators are used in cables of electric cars or in coils for the improvement of resins [40].
- By doping the polymers with the black carbon or CNTs results in the polymers that conducts electricity. These conductive polymers can be used in the electronic devices for the electrostatic shielding [40].
- Polymers doped with the nanoparticles for example silver nanoparticle are used in the medicine industry and for hygiene purposes [40].

1.5.3 Metal matrix nanocomposites

These types of composites have improved thermo-mechanical properties. Matrix can be a ceramic fibers such as SiC or Al_2O_3. By reinforcing the metal with such type of fibers, an improvement showed up in the aforementioned properties. These metal matrix nanocomposite have the potential in the aerospace and the automotive industry due to the

elevated heat resistance, good thermal conductance, low density, hardness and manageable thermal expansion [41].

1.5.4 Ceramic nanocomposites

In the ceramic nanocomposites a special concern lies in the synthesis of micro/nano materials in the controllable manner by changing its composition. Apart from the synthesis, a special concern lies in the application of coating nanomaterials and for the functionalization of surfaces of the material. Ceramic nanomaterials are considered as brittle materials and the main objectives of these materials are to improve the thermal and mechanical properties as well as to improve the super-plasticity. By coating the ceramic materials with the nanopowders the sintering temperature reduces and there is also a decrease in the consolidation time and not only this, it also strengthen the material in less time, develops a new technique for the synthesis of high purity samples and save a lot of money and time. To synthesize the ceramic nanopowders a gas or a liquid phase synthesis can be used. A gas phase synthesis is preferable if a non-oxide powders are used and if the oxide powders are used a liquid phase synthesis or a sol-gel technique can be used [40, 42].

1.5.5 Synthesis of composites

Traditionally the synthesis of composites need a great effort in crushing, grinding and blending. By following this method a submicron size composite powder can be synthesized. Chemical method proves to be a more precise and relevant method for the production of composite. The main advantages of chemical method is the reduction of the particle size to the nano level and a homogeneous material can be achieved. For example precursor material is obtained by using the aqueous precipitation of salt which is further treated by thermochemical method to synthesize the composite [43]. Solution dispersion synthesis technique is used to add multi walled carbon nanotubes (MWCNTs) to the polymer. The direct wrapping of MWCNTs doesn’t occur in polymers so the organic solvent is used to dissolve the MWCNTs and polymer. Covalently attached polymers and single wall carbon nanotubes (SWCNTs) are considered to be water soluble and the electrical properties changes by the covalent attachment. These type of composites have an application to fabricate near-infrared devices [44].

A huge interest in the past few years has been shown in the synthesis of ferrite nanoparticles/graphene oxide composites. Their applications vary in the field of environmental protection such as for the detection of heavy metals in contaminated water, soil and for the detection of toxic gases (NH_3, CO_2) in the environment and also in the field of biomedical. D F Zhao [45] have successfully synthesized the semiconductor/graphene nanocomposite. GO is used as a precursor which is then reduced to graphene. Two different synthesis routes have been proposed for the synthesis of semiconductor/graphene nanocomposite. The first route proposes the in situ growth of semiconductor particles on the graphene, which is considered as a one step process in which GO is also reduced to graphene. The second method proposes the mixing of both materials in the ultra-sonication bath followed by further treatment of the reduction of graphene oxide using photocatalytic irradiation [45]. Several other methods have also been reported for the synthesis of ferrites nanoparticles/graphene oxide nanocomposites including 1) precipitation of ferrite nanoparticles on graphene oxide in water, 2) ferrite nanoparticles are mixed with graphene oxide in the polar solvent using solvothermal synthesis or thermolysis, 3) ferrite nanoparticles are covalently attached with the graphene oxide [46]. Y Xiao [47] have successfully synthesized the cobalt ferrite/graphene nanocomposite by mixing the cobalt ferrites and graphene in water and are treated ultrasonically followed by the annealing at different temperatures. By using ultra-sonication method, a good dispersion of ferrites and graphene was obtained. High carbon quality, optimization of ferrite/graphene interface and the graphene conductivity was improved by annealing [47].

1.6 Nanoparticles based Sensors

Sensors based on magnetic nanoparticles (MNPs) have several advantages including increased sensitivity, low limit of detection, high signal to noise ratio and a decreased analysis time. MNPs are used in the number of different ways for sensing application. Either MNPs have direct contact with the sensors or they are combined with the transduction material which are dispersed in the solution[48]. These sensors are classified by their transduction principles such as electrochemical sensor [49], optical sensor [50], piezoelectric sensor [51]and magnetic field based sensor [20].

1.7 Electrochemical sensor

Sensors which transform the effect of the electrochemical interaction analyte-electrode into a useful signal are known as electrochemical sensors. The interaction between the analyte and the electrode generates an electrochemical signal in the form of current, voltage or impedance. This transmitted signal can be measured using an electrochemical device. The surface activity of the electrodes can be improved by coating the electrode with different materials for required application. Electrochemical devices have several advantages of being low cost, robust, highly sensitive, selective, easy to carry and operate [52].

These electrochemical devices have much potential in environmental, medical and in pharmaceutical industry. According to the working principles, the electrochemical sensors are classified as capacitive, amperometric, volumetric, resistive and potentiometric [53]. By using the magnetic nanoparticles on to the surface of the electrode enhances the sensitivity of the electrochemical device. The voltammetry technique is mostly used for the electrochemical sensors for the detection of the signals coming from the interaction between analyte and the electrodes [54, 55].

Heavy metals are contaminants that are present in the environment and are linked with certain chemical species. Detection of these contaminants is very important because they are highly toxic and can cause very serious problems to human health. Certain techniques have been proposed for the elimination of these metal ions such as atomic absorption spectroscopy [56], inductively coupled plasma mass spectroscopy [57] etc. These techniques are not useful as these techniques required trained staff and are expensive and time consuming. To overcome these problems electrochemical sensors are used for the detection of such metal ions from the environment. To increase the sensitivity of the electrochemical sensors different materials are used to coat the electrodes such as ferrite nanoparticles, ferrite/GO composite etc. [58, 59].

Iron (III) oxide exhibits super paramagnetic property and shows biocompatibility to the biological compounds such as antibodies and enzymes. This chemical compound can easily be prepared and due to such properties it can be used as a biosensor. Sometimes aggregation results when Fe_3O_4 is mixed with biological solution due to its

high surface area to volume ratio and attraction due to magnetic bipolar. This aggregation problem can be solved by functionalization of magnetic nanoparticles and it also intensify biocompatibility [60]. A wide variety of functionalized nanoparticles can be used such as iron (III) oxide decorated on rGO [61], $AuFe_3O_4$ composite nanoparticles [62] and core-shell $AuFe_3O_4$ [63].

1.7.1 Working principle of Electrochemical Sensor

Electrochemical sensor works by reacting with the analyte and generating an electrical pulse. This electrical pulse is proportional to the concentration of the analyte. A distinctive electrochemical sensor consists of a working electrode, reference electrode and a counter electrode separated through an electrolyte [49, 64]. A typical potentiostat for the detection of the analyte is shown in Figure 1.6.

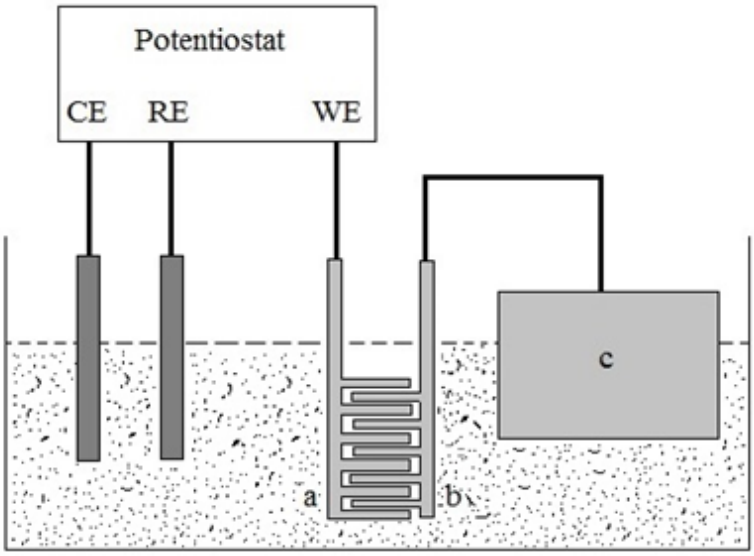

Figure 1.6. A typical electrochemical sensor for the detection of heavy metals. (a) Working electrode 1 (b) Working electrode 2 and (c) Macro electrode

A potentiostat is a device used to control the potential difference between the working electrode (WE) and a reference electrode (RE). Current is measured between the working electrode and a counter electrode (CE). Basically a potentiostat operates with a three cell system in an electrochemical cell. All these electrodes are dipped in the electrolyte of an electrochemical cell. Figure 1.6 shows a schematic of an electrochemical sensor used for the detection of heavy metals. The working electrode used is the interdigitated electrode (IDE) explained in the next section.

1.8 Interdigitated electrode (IDE)

An interdigitated electrode (IDE) is a device consisting of two interconnected comb shaped arrays of electrodes as shown in figure 1.7. These electrodes are fabricated on a substrate such as glass, silicon, fiber etc by using lithography, screen printing and sputtering [65-67].

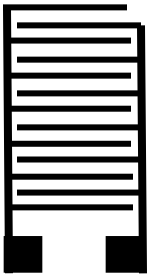

Figure 1.7. Interdigitated electrode device with their contact pads

For enhancement of sensitivity and selectivity, several geometries of microelectrodes have been assessed in the past few years [68]. Among all the geometries, IDEs has taken considerable interest. In the interdigitated arrays of electrodes, redox cycling takes place. The oxidation takes place at one electrode while the reduction takes place at the other electrode. This redox cycling takes place when both electrodes can be potentiostated, so species that are generated at one electrode can diffuse to the other electrode and from there they diffuse back to their original form. This redox coupling results in the increment of current [68, 69].

IDEs are largely used for several sensor applications such as in gas sensor [70], heavy metals detection [71], biosensors [72] and humidity sensor [73]. Electrical signals generated by the analyte used as a sensing material is frequently detected using IDEs. As described earlier, IDEs are used for better sensitivity and selectivity. Sensitivity is attributed to the gap between the fingers of the electrodes and decrease in the gap increases the sensitivity of the IDE. The small sizes of the IDE not only increases the sensitivity but decreases sample volume.

Electrochemical detection is vastly used for the determination of analyte at trace level. It offers selectivity as well as direct method to determine the analyte. Electrochemical measurements can be carried out using IDE operated in a single or dual

mode. Cyclic voltammetry (CV) is the technique used to characterize the IDE in single or dual mode. A bipotentiostat is used in dual mode to handle the two working electrodes. One of the electrode is referred to as a collector (fixed potential) while the other electrode as a generator (potential sweep).

When the IDE is operated in single mood, only one electrode is potentiostated. Dual mode has an advantage of higher current and redox cycling at the very close fingers [68].

Chapter 2

Experimental

2.1 Materials

$Ni(NO_3)_2.6H_2O$ (99.9% purity, Merck), $Mg(NO_3)_2.6H_2O$ (99.9% purity, Sigma Aldrich), $Fe(NO_3)_3.9H_2O$ (99.9% purity, Sigma Aldrich), NaOH (99.9% purity, Sigma Aldrich), Graphene Oxide (Graphene market, USA), hydrazine hydrate were used for the synthesis of ferrites and ferrite/rGO nanocomposite. Ultrapure water of conductivity 0.35 S/m was used. All materials used were of analytical grade.

2.2 Synthesis of $Ni_{0.5}Mg_{0.5}Fe_2O_4$ ferrites

Co-precipitation route has been used for the synthesis of $Ni_{0.5}Mg_{0.5}Fe_2O_4$ with stoichiometric amount taken as 0.5:0.5:2. Hydrated nickel nitrate $Ni(NO_3)_2.6H_2O$ (18.9mg), magnesium nitrate $Mg(NO_3)_2.6H_2O$ (16.67mg) and iron nitrate $Fe(NO_3)_3.9H_2O$ (525.2mg) were taken as the initial precursors for the preparation of $Ni_{0.5}Mg_{0.5}Fe_2O_4$ nanoparticles. These initial precursors were added individually to separate beakers containing 100ml ultrapure water. A magnetic stirrer was put in each beaker that were placed on hot plate for 15minutes to form dispersions through continuous stirring. These three dispersions were mixed in a single beaker and 3M sodium hydroxide (NaOH) was added drop by drop to neutralize this solution while stirring. This overall reaction was carried out at 85 ^{O}C for 45minutes. Once the reaction was completed, the solution obtained was kept for one night to settle down the precipitates. The excess water was removed and the precipitates obtained were washed several times with distilled water to obtain the pH of 7. This washing process continued until all the sodium and nitrate ions were removed from water. The product obtained after washing was dried in an oven at 110 ^{O}C for one night to remove any moisture. The dried product was then grounded in mortar and pestle to obtain the fine powder. The fine powder obtained was then sintered at 400 ^{O}C for 4 hours withholding time to obtain $Ni_{0.5}Mg_{0.5}Fe_2O_4$ nanoparticles [74-76]. Figure 2.1 shows the flow chart of this whole synthesis process.

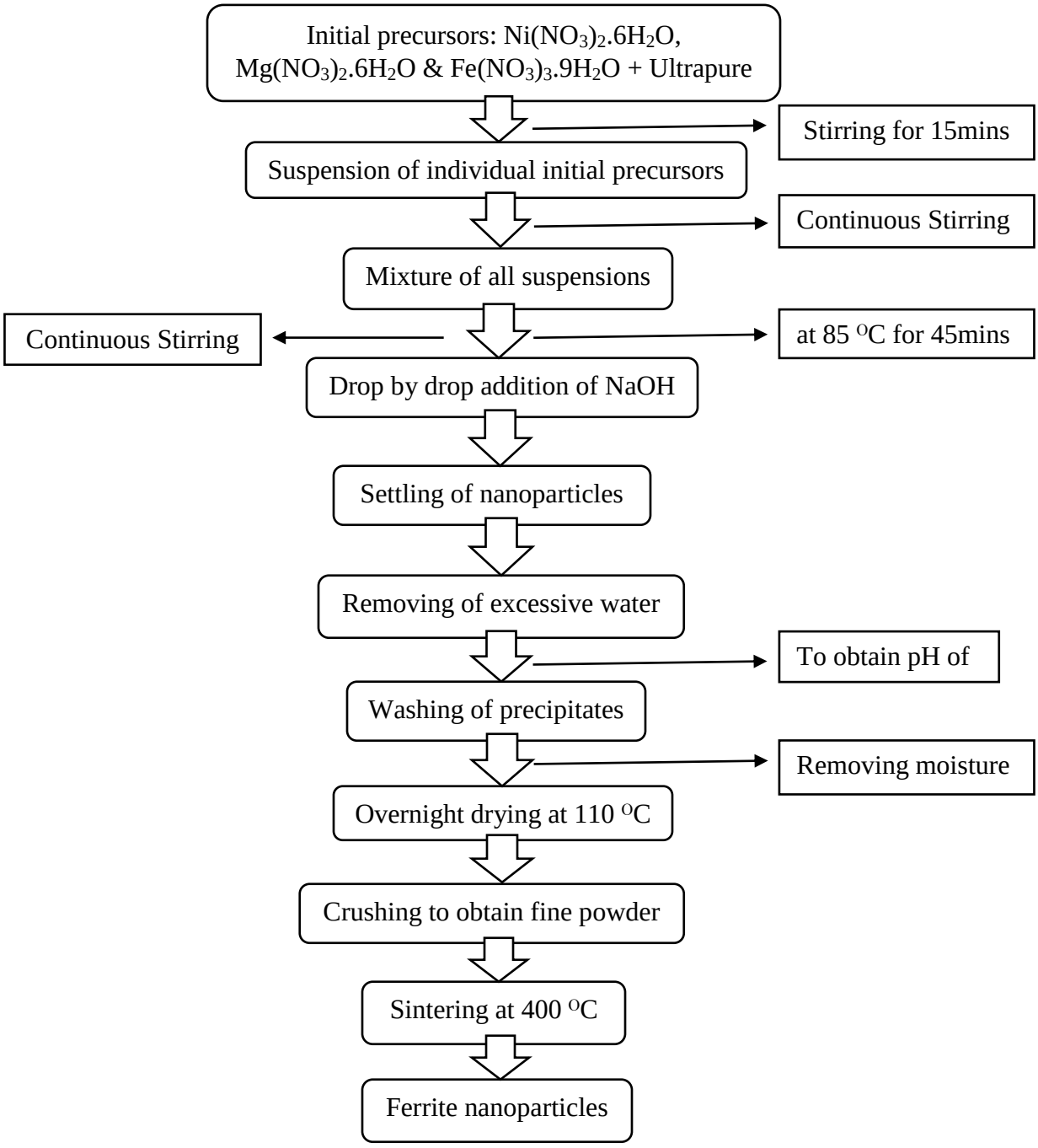

Figure 2.1 Flow chart for the synthesis of ferrites by co-precipitaion route

2.3 Synthesis of $Ni_{0.5}Mg_{0.5}Fe_2O_4$/rGO nanocomposite

Composite of nickel-magnesium ferrite nanoparticles ($Ni_{0.5}Mg_{0.5}Fe_2O_4$) and reduced graphene oxide (rGO) was synthesized through ultra-sonication method. 2mg of GO was added to 5ml ultrapure water in a graduated beaker and placed in an ultra-sonication bath. After 30 minutes of sonication, 5mg $Ni_{0.5}Mg_{0.5}Fe_2O_4$ ferrites were added to this solution and further sonication for 30 minutes was performed. After sonication, 1ml of hydrazine hydrate was added to the solution for the reduction of GO and further sonication was done for 60 minutes. The solution was washed in centrifuge by using distilled water and the product obtained was then annealed at 250^{O}C in nitrogen atmosphere for 60 minutes at the heating rate of 10 ^{O}C min^{-1} [47, 77]. Flow chart of this synthesis process is shown n Figure 2.2.

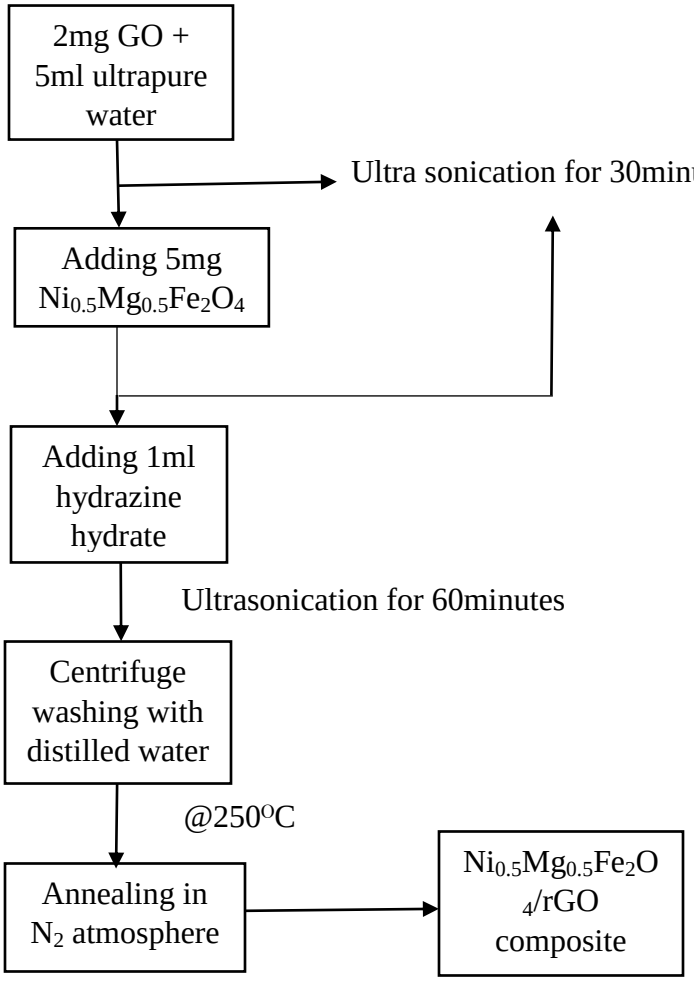

Figure 2.2 Flow chart for the synthesis of composite

2.4 Fabrication of interdigitated electrode (IDE)

To fabricate interdigitated electrodes, single sided copper clad board (PCB) of dimensions 12” x 6” x 0.06” inches (~ 300mm x 150mm x 1.5mm) was used. The initial thickness of copper layer laminated on the FR4 composite material was 0.035mm. The appearance of the copper board was dull as it had gathered a very thick oxide layer that was needed to be removed (Figure 2.3). Super fine sandpaper with 600 grit size was used to slightly scrub the surface under running water until bright metallic look of copper appeared (Figure 2.4). The surface was further washed with ultrapure water and ethanol. After drying, the board was stored in an air tight chamber to avoid any further oxidation.

Figure 2.3 Copper Board with thick oxide layer

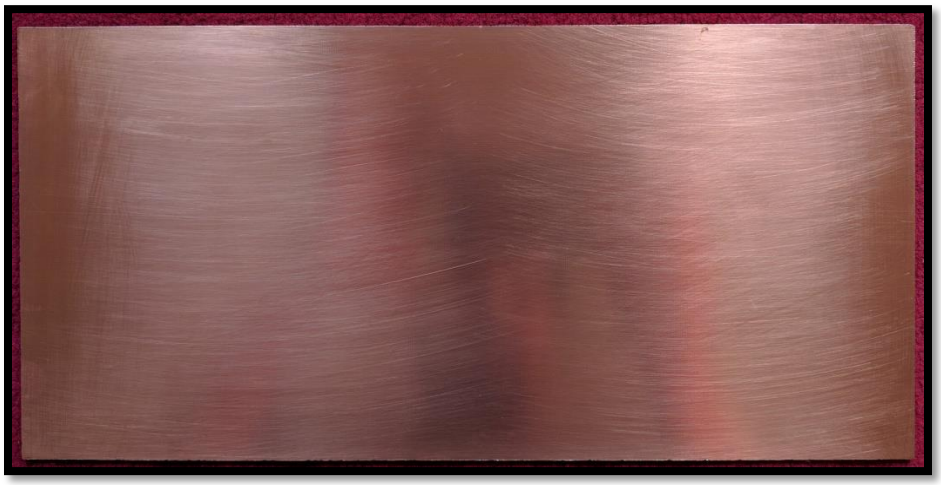

Figure 2.4 Cleaned Copper Board

The next part included the designing of interdigitated electrode (IDE) template, which was created by using Autodesk Autocad 2015 software. The actual CAD design and dimensions of the IDE are given as (Figure 2.5 and 2.6 respe

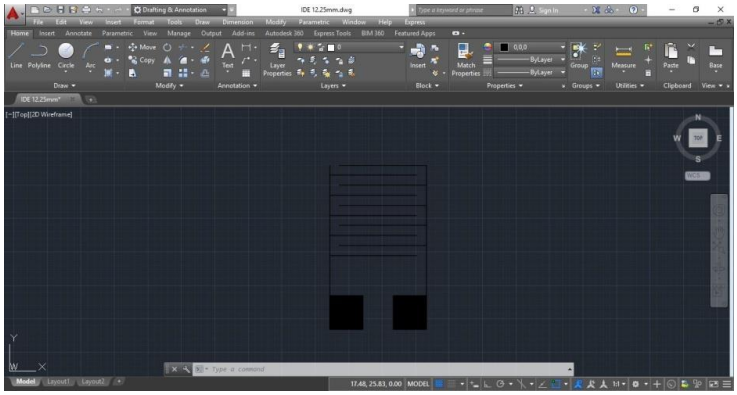

Figure 2.5 AutoCAD Design of IDE

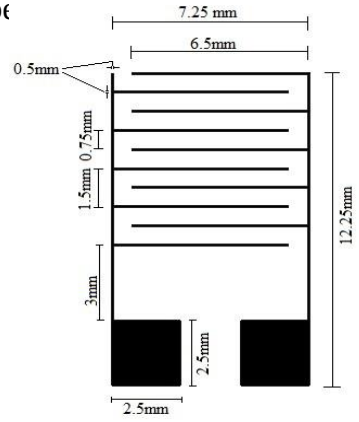

Figure 2.6 Dimensions of IDE

The design was scanned onto a transparent film in order to make a mask (Figure 2.7). This mask was used to transfer the design onto the copper board by screen printing technology. PVC ink was used to make this design on the copper board (Figure 2.8). The designed copper board was etched by using laboratory grade ferric chloride ($FeCl_3$), that removed all the copper except the part that was under the PVC ink design (Figure 2.9). By using acetone the ink was removed from the copper board, leaving behind the designed IDEs (Figure 2.10).

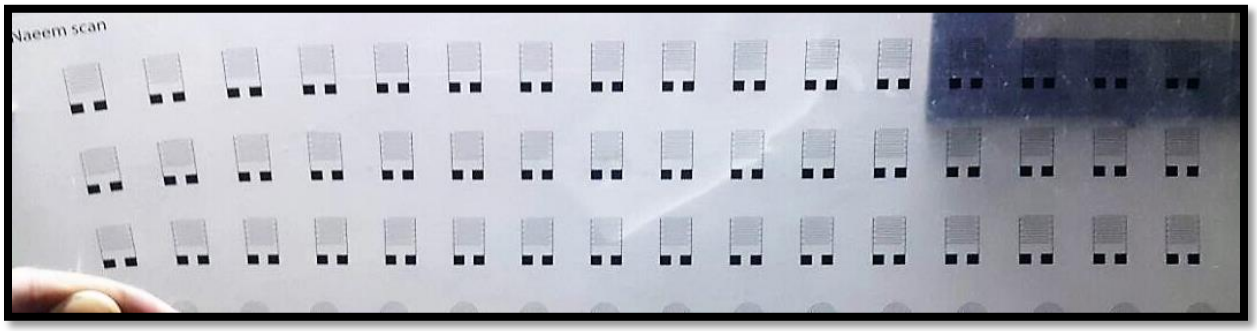

Figure 2.7 Transparent film (mask fabrication)

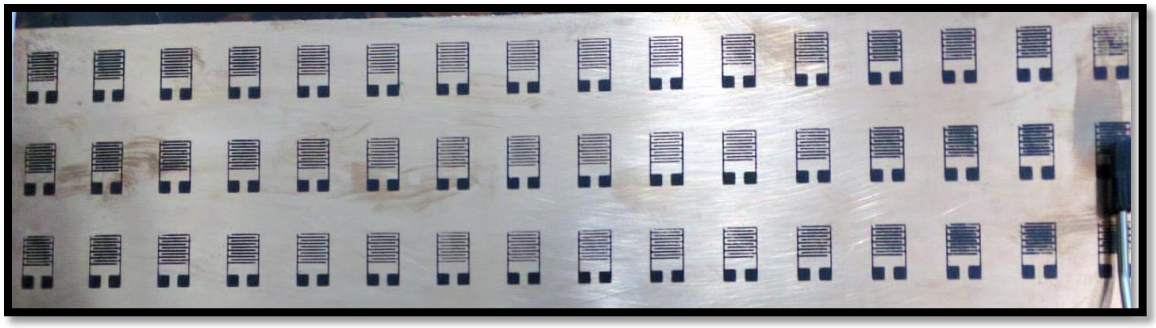

Figure 2.8 Copper board with IDE design using PVC ink

Figure 2.9 Etched copper board

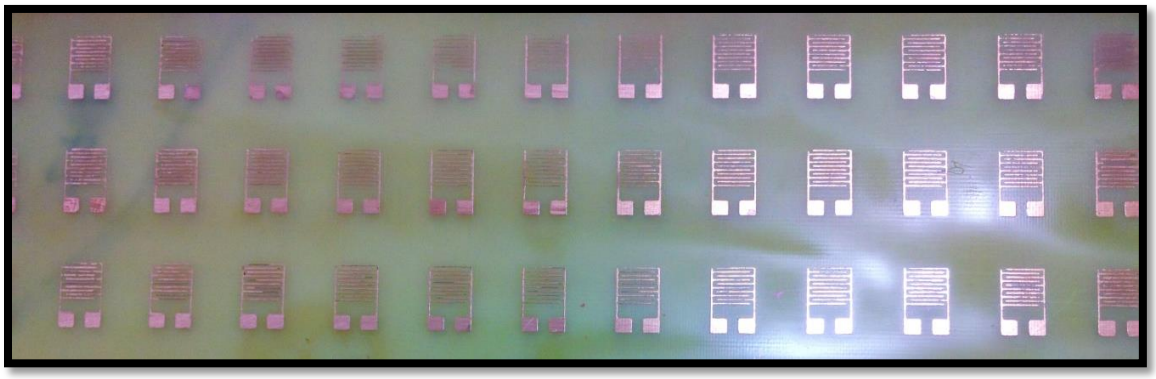

Figure 2.10 The designed copper based IDEs

PCB (printed circuit board) cutter was used to finely cut all the fabricated IDEs, so that individual interdigitated electrode could be obtained for sensing purposes (Figure 2.11). All the IDEs were tested by digital multimeter (DMM) to check the connectivity and the short circuited ones were discarded. The remaining IDEs were further analyzed under an optical microscope (Figure 2.12) to check the exact dimensions and half printed or disconnected wings based IDEs were discarded also. Only, IDEs resembling to original CAD design dimensions were kept for sensing applications. These IDEs were further cleaned through the same procedure as mentioned above by using 600 grit super

fine sand paper, ultrapure water and ethanol. The final thickness of copper layer measured was 0.025mm, rest being removed through the cleaning process. All the usable IDEs were stored in an air tight chamber to prevent oxidation or any impurity that may stick to them.

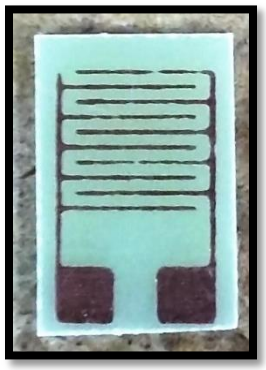

Figure 2.11 Single IDE

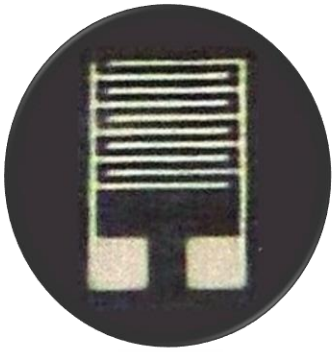

Figure 2.12 Optical microscope image of a single IDE

2.5 Dispersions of Sensing Materials

Dispersions of $Ni_{0.5}Mg_{0.5}Fe_2O_4$, GO and $Ni_{0.5}Mg_{0.5}Fe_2O_4$/rGO were prepared individually in de-ioized water. 8mg $Ni_{0.5}Mg_{0.5}Fe_2O_4$ was dispersed in 0.392ml de-ionized water to make 2% w/w $Ni_{0.5}Mg_{0.5}Fe_2O_4$ in de-ionized water. Similarly 2% w/w GO and 2% w/w $Ni_{0.5}Mg_{0.5}Fe_2O_4$/rGO nanocomposite dispersions were prepared (Figure 2.13)

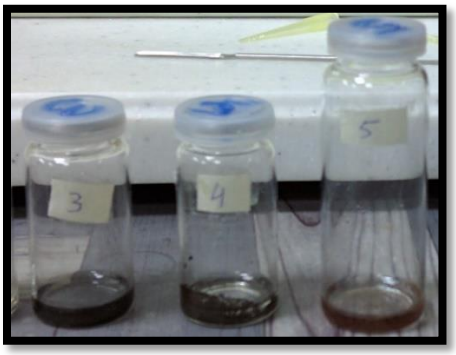

Figure 2.13 Dispersions of $Ni_{0.5}Mg_{0.5}Fe_2O_4$, GO and $Ni_{0.5}Mg_{0.5}Fe_2O_4$/rGO

2.6 Fabrication of Sensor

To fabricate electrochemical sensor for detection of Pb^{2+} ions, a 20µl amount from the dispersions of $Ni_{0.5}Mg_{0.5}Fe_2O_4$, GO and $Ni_{0.5}Mg_{0.5}Fe_2O_4$/rGO nanocomposite

were drop casted on different IDEs. These modified IDEs were left to dry at room temperature. After complete drying in 2 hours, a thin layer of $Ni_{0.5}Mg_{0.5}Fe_2O_4$ (Figure 2.14a), GO (Figure 2.14b) and $Ni_{0.5}Mg_{0.5}Fe_2O_4$/rGO (Figure 2.14c) got deposited on the different IDEs.

These film deposited IDEs were used as a working electrode in the three electrode system of potentiostat.

(a) (b) (c)

Figure 2.14 Film Deposited IDEs

2.7 Electrochemical Characterization Setup

Cyclic voltammetry was performed using Gamry potentiostat (G750) shown below (Figure 2.15).

Figure 2.15 Gamry potentiostat G750

A three electrode system was used to perform cyclic voltammetry. IDE was used as a working electrode (Figure 2.16a) and saturated calomel electrode (Figure 2.16b) was used as a reference electrode. Graphite rod (0.242” × 6”) was used as a counter electrode (Figure 2.16c). Glass membrane (Figure 2.16d) was used to hold reference electrode. Gamry euro cell kit (990-00196) item # 13 count 1 was used (figure 2.16e).

(a) (b) (c)

(d) (e)

Figure 2.16 (a) Working electrode, (b) Reference electrode, (c) Counter electrode, (d,e) gamry cell euro kit

Schematic of the electrochemical analysis of film deposited IDEs (figure 2.17). A scan rate of 100mV/s was used with a potential window ranges from -600mVto 0mV.

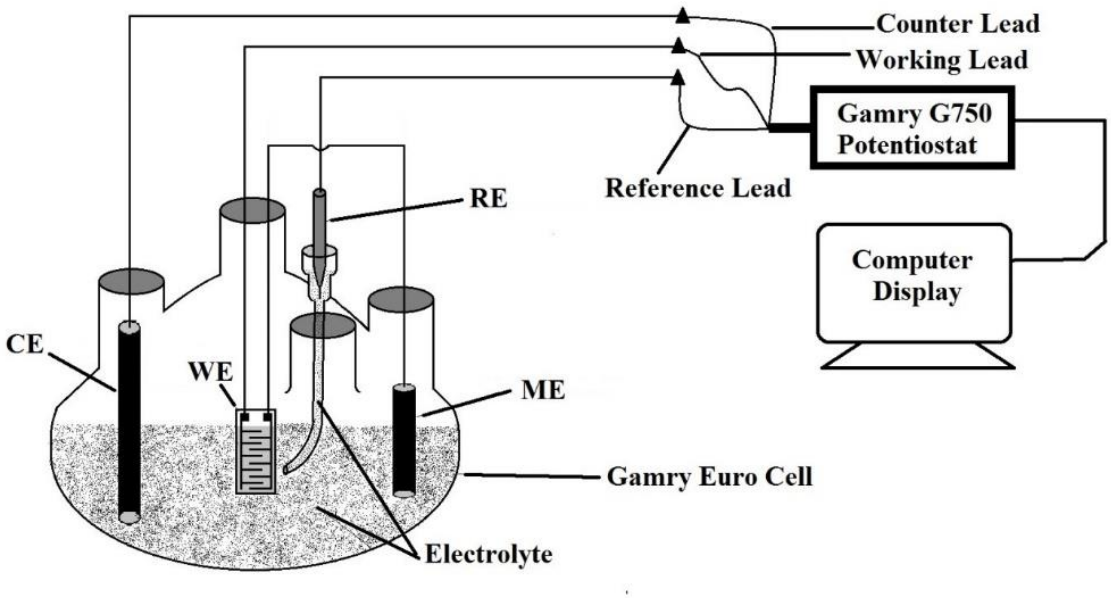

Figure 2.17 Schematic of the CV, EIS and LSV performed for the detection of heavy metals

Chapter 3

Results and Discussion

3.1 Characterization Techniques

3.1.1 Scanning Electron microscope (SEM)

Scanning electron microscopy is a technique used for the characterization of materials surface. SEM renders an image with the magnification of about 10x-300,000x. It not only provides topographical data but also render surface composition of the sample.

In SEM, an electron beam is used to scan and examine the specimen's surface. The scanning of electron beam over the specimen surface results in the reflected or backscattered electron beam, which is collected and then displayed on a cathode ray tube (CRT). The image generated on screen shows the features of the specimen surface [78].

A very little amount of sample is required for SEM. In most cases the sample is conducting and if the sample is an insulator, it needs to be coated with a thin film of some conducting metals such as gold, carbon etc. Nonuniform coating leads to distortion or agglomeration of the coating material. If x-rays analysis performed on this nonuniform coated surface, x-ray peaks produced in the posited material must be removed or corrected. SEM can also be performed on insulating samples that are not coated. These samples can be studied on low beam voltages (<2eV) with low resolution [79].

3.1.2 X-Ray Diffraction (XRD)

XRD is a technique used to identify the materials crystalline phases and to measure the different properties of the materials structure. These properties include the grain size, defect structure and phase composition. Thin films and multilayers are also studied under XRD for their thickness, and amorphous materials are also taken under consideration for their atomic arrangement.

XRD is useful for in situ studies because it is a non-destructive technique. Materials consists of multilayers, studied using XRD provides quantitative and complete information of their measured intensities. XRD is also used to study the materials which

consists of elements, but XRD is much sensitive to the high Z- element then to the low Z-element, because in high Z-element the intensities of the diffracted beam is much high. As a result, XRD sensitivity depends upon the material of interest. Surface sensitivities less than 50Å thickness can be accomplishable using equipment used in lab, and the sensitivity of much thinner surfaces can also be achievable using synchrotron radiation because of its much higher intensity.

Transmission electron microscope (TEM), Low Energy Electron Diffraction (LEED), Reflection High Energy Electron diffraction (RHEED) and neutron diffraction can be used as an alternatives to the XRD. LEED and RHEED are used only to scan the surface of the materials, not for the scan of bulk materials. Neutron diffraction is a little bit different as compare to XRD. XRD sources are much stronger than neutron diffraction, however for magnetic moments, neutrons sensitivity is much better than XRD. If the material is in bulk and is magnetic in nature, then neutron diffraction is preferable then low-Z materials.

When an x-ray hits the atom, it will be scattered entirely in the atom in all directions. If the atoms are arranged periodically, then the scattered rays cancel out each other effect. The strongest scattered x-rays are considered those which arrives in phase at the detector. This results in a relationship known as Bragg's law [80].

$$\lambda = 2d\sin\Theta$$

Where,

λ is x-ray wavelength

d is spacing between lattice planes

Θ is angle of incidence

An atomic plane has its unique miller indices

3.1.3 Cyclic Voltammetry (CV)

Cyclic voltammetry (CV) is a standard tool in electrochemistry which is used for the determination of electrode reaction mechanisms, standard electron transfer rate constants, and diffusion coefficients [81]. In a CV technique potential applied, through a three electrode potentiostat, to an electrochemical cell is scanned and the resulting cell current is output vs. potential. A typical three-electrode cell for CV characterization includes a working electrode, a reference electrode, and a counter electrode (Figure 3.1). The potentiostat controls the potential of the working electrode vs. the reference electrode, while compensating for as much of the cell resistance as possible [82]. Counter (or auxiliary) electrode is used to complete the electrical circuit.

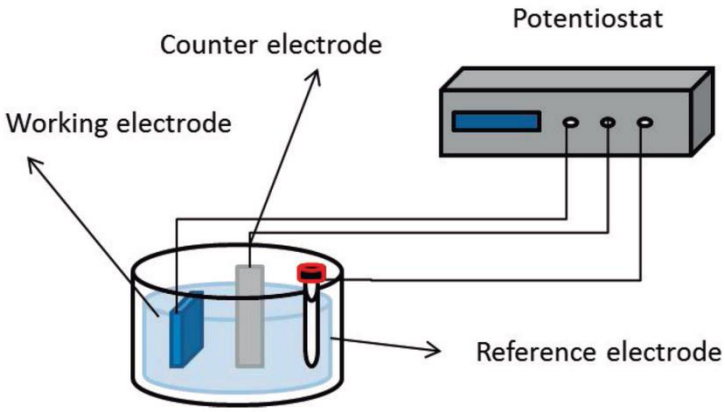

Figure 3.1 Schematic of a typical CV three electrode cell [83]

In cyclic voltammetry, the information about the analyte is obtained by measuring the Faradaic current as a function of the applied potential. The response of the current over a potential range is measured, starting at an initial potential value and the potential is varied in a linear manner up to a limiting value (final potential value). As this final value is reached, the direction of the potential scan is reversed; after which the scanning takes place over the same potential range in the opposite direction (that is why the term “cyclic” is used). As a result, the species generated by oxidation on the forward scan are reduced on the reverse scan [84]. Scan rate (mV/s) determines the time taken to sweep the range.

Cyclic voltammogram showing important parameters that can be obtained from CV of a reversible redox couple is shown in Figure 3.2. The parameters obtained include

peak potentials (E), peak currents (i) and the potential difference ΔE between the reduction (R) and oxidation (O) peaks. From these parameters, the electron transfer mechanism of the electrode gets clarified to an extent [85].

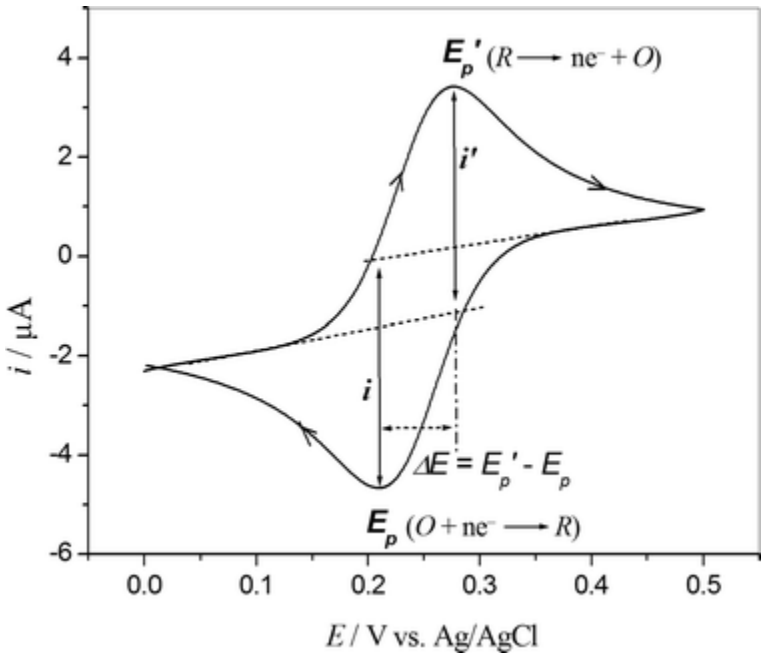

Figure 3.2 A typical cyclic voltammogram showing of a reverse redox couple important parameters [85]

3.1.4 Electrochemical Impedance Spectroscopy

Electrochemical impedance spectroscopy (EIS) is a technique used to investigate charge transfer, transport of ions, and processes related to adsorption on metals and semiconducting electrodes [86]. In EIS measurements, impedance dependent on a frequency is obtained when a sinusoidal alternating potential signal is applied to the tested system over a range of frequencies. These measurements are carried out in an electrolyte (i.e., a conducting solution) [87]. The EIS technique recognizes any process that tends to change the conductivity of the system. The effects, which include enhancement in electron transfer and sensitivity, of different layers and coatings deposited on an electrode can be identified using EIS. EIS is also used to measure other key parameters of any electrochemical system under investigation that include charge-transfer resistance, double layer capacitances and current densities [88].

The data obtained from EIS is analyzed by fitting it to an equivalent electrical circuit model. The impedance data is presented by plotting two different graphs; the Nyquist plot (Figure 3.3a) and the Bode plot (Figure 3.3b). Nyquist plots the real component (Z) on x-axis and the imaginary component (Z') on the y-axis. For Nyquist plot, graph doesn't display the frequency for data collected, hence Bode plot is often used to display the same data. Bode plot shows the relation between the frequency (f) with phase angle (Θ) and the equivalent impedance [89].

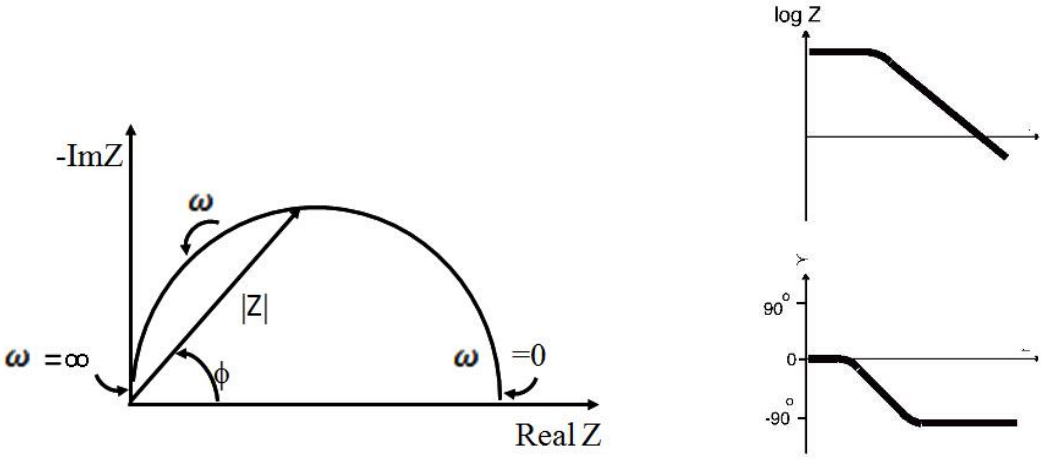

(a) *(b)*

Figure 3.3 Nyquist plot (a) Bode plot (b) for a simple electrochemical system [89]

3.2 X-Ray diffraction analysis (XRD)

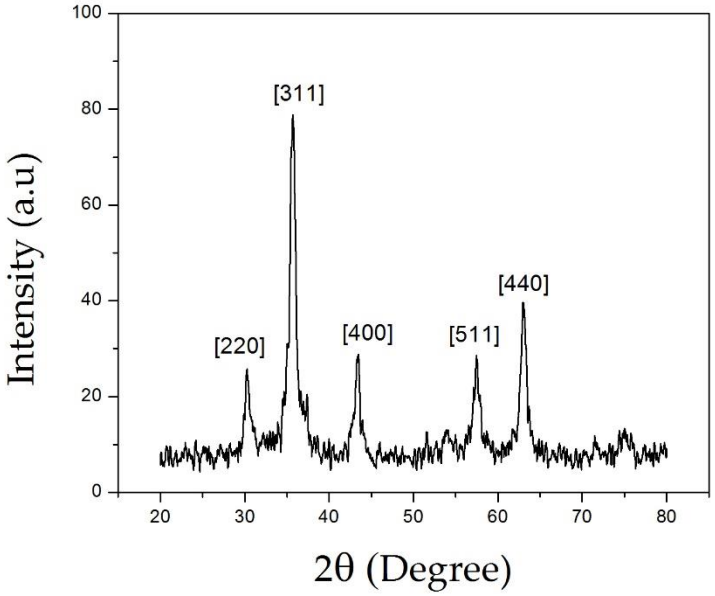

Figure 3. 4 XRD plot of $Ni_{0.5}Mg_{0.5}Fe_2O_4$

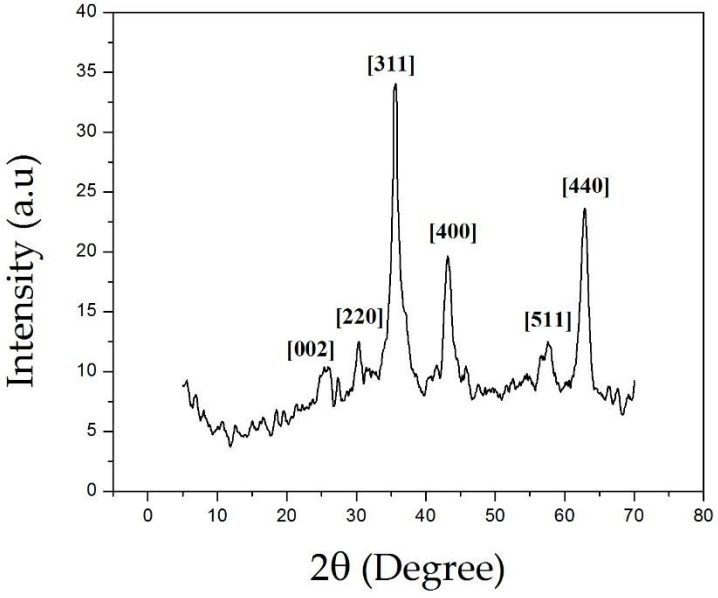

Figure 3.5 XRD plot of $Ni_{0.5}Mg_{0.5}Fe_2O_4$/rGO

XRD analysis was performed using STOE & Cie GmbH manufacturer machine operating at 40mA and 40kV. XRD graphs of $Ni_{0.5}Mg_{0.5}Fe_2O_4$ and $Ni_{0.5}Mg_{0.5}Fe_2O_4$/rGO

are shown in figures (3.4 and 3.5). The 2Ɵ range was kept from 20-80 degrees. Figure 3.4 shows all the related peaks for the spinel structure. All the peaks were also present in case of $Ni_{0.5}Mg_{0.5}Fe_2O_4$/rGO with the rGO peak at [002]. The presence of rGO peak shows the successful synthesis of $Ni_{0.5}Mg_{0.5}Fe_2O_4$/rGO nanocomposite.

3.3 Scanning Electron Microscope (SEM)

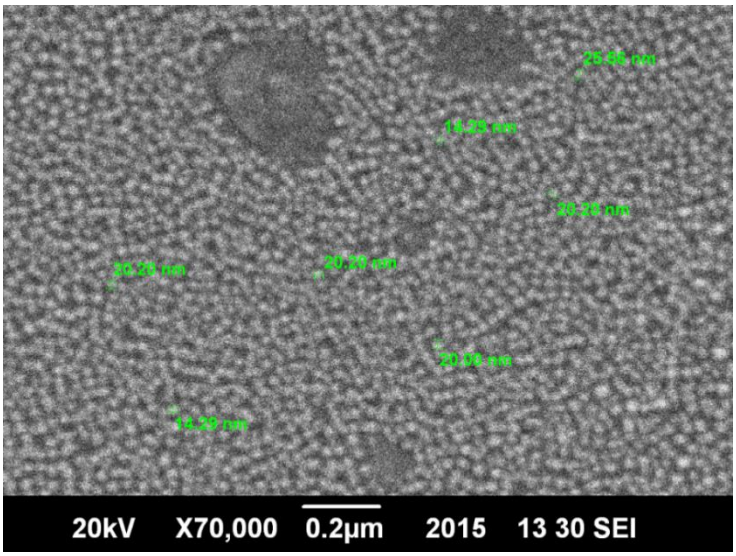

Figure 3.6 SEM image of $Ni_{0.5}Mg_{0.5}Fe_2O_4$

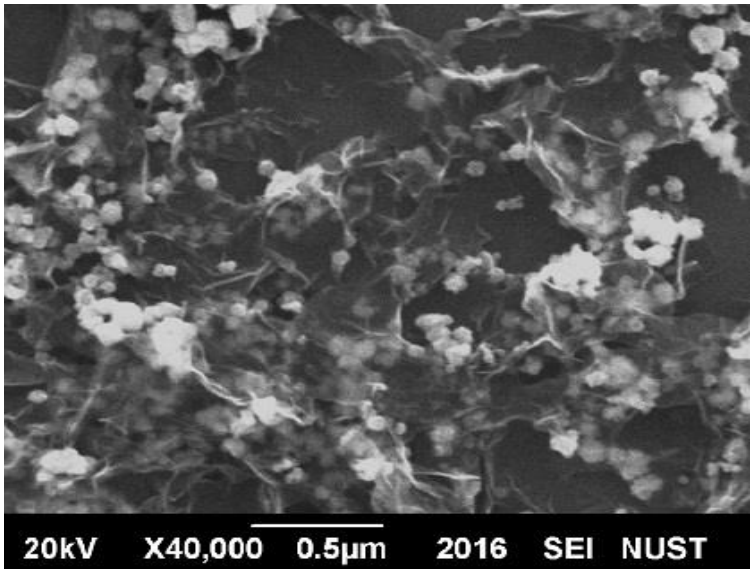

Figure 3.7 SEM image of $Ni_{0.5}Mg_{0.5}Fe_2O_4$/rGO

Jeol corporation Japan manufacturer based scanning electron microscope (model# Jeol JSM-6490A) was used for the analysis of samples. SEM analysis was performed by

dispersing the very little amount of ferrites and nanocomposite in the ultrapure water followed by the gold coating. Gold coating was done (Jeol JFC-1500) by ion sputtering machine because the samples are not conductive. Figure 3.6 and 3.7 shows the SEM images of $Ni_{0.5}Mg_{0.5}Fe_2O_4$ and $Ni_{0.5}Mg_{0.5}Fe_2O_4$/rGO. Figure 3.6 shows that $Ni_{0.5}Mg_{0.5}Fe_2O_4$ nanoparticles are homogeneously and well dispersed. The average particle size is ranging from 14.29nm to 25.56nm. Figure 3.7 shows the rGO decorated with $Ni_{0.5}Mg_{0.5}Fe_2O_4$.

3.4 Cyclic Voltammetry (CV)

3.4.1 Electrochemical characterization of IDEs in 0.1M KOH

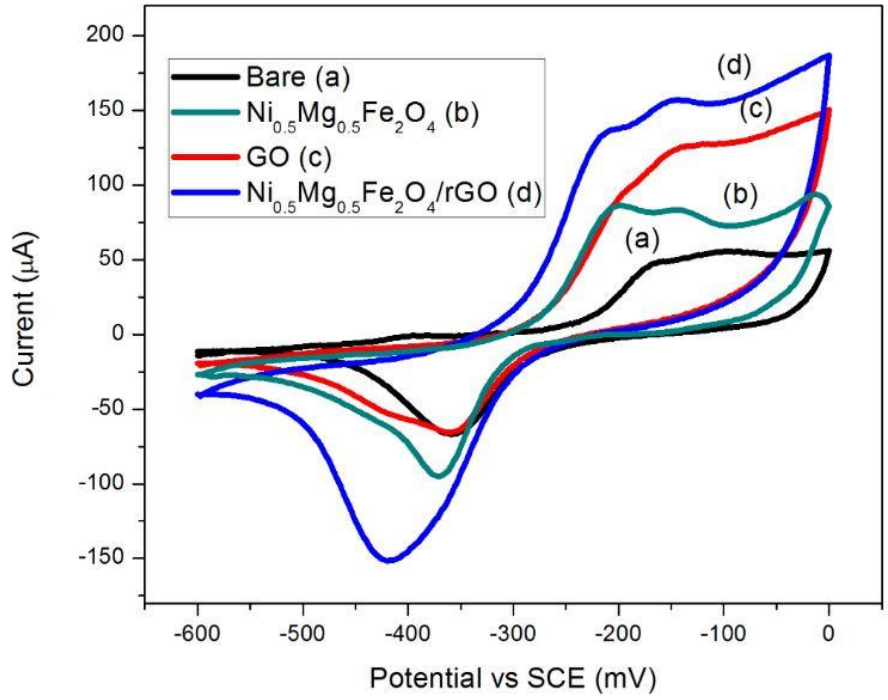

Figure 3.8 Cyclic voltammogram of bare, reduced graphene oxide, nickel-magnesium ferrite, composite in 0.1M KOH.

Figure 3.8 shows the cyclic voltammograms of bare and modified IDEs in 0.1M KOH. The minimum current is shown by the bare IDE while the Ferrite/rGO composite shows the maximum current. By depositing Ferrite ($Ni_{0.5}Mg_{0.5}Fe_2O_4$) film on the IDE the current increases because the surface area of the IDE increases and its adsorption capability also increases. GO has a better electronic properties, hence IDE modified with GO shows an enhanced current then IDE modified with ferrites or bare IDE due to fast

electron transfer kinetics. By combining the $Ni_{0.5}Mg_{0.5}Fe_2O_4$ with rGO the electron transfer kinetics, the electrode surface area and the adsorption capability increases. So the combination of $Ni_{0.5}Mg_{0.5}Fe_2O_4$ and rGO shows up the maximum response. The peak currents (I_p red and I_p ox) and the charge 'Q' (Area under the curve) is shown in table

IDE	I_p red (µA)	-I_p ox (µA)	Q (C)	ΔEp (V)
Bare	55.96	66.69	93.20	2.82E-01
$Ni_{0.5}Mg_{0.5}Fe_2O_4$	94.04	95.32	162.4	1.74E-01
GO	150.5	65.62	260.3	2.60E-01
$Ni_{0.5}Mg_{0.5}Fe_2O_4$/rGO	186.8	151.4	350.7	2.76E-01

Table 3.1 Peak cathodic and anodic currents, Area under the curve (Q) and peak potential separation (ΔEp)

Table 3.1 shows the peak reduction current, peak oxidation current, charge (Q) and peak potential separation (ΔEp). The area under the curve (Charge) is also increasing by modifying the IDE with nanomaterials. $Ni_{0.5}Mg_{0.5}Fe_2O_4$/rGO shows maximum charge due to the fast electron kinetics and more surface area for charges to interact with the IDE.

3.4.2 Detection of 10ppb lead using bare and modified interdigitated electrode

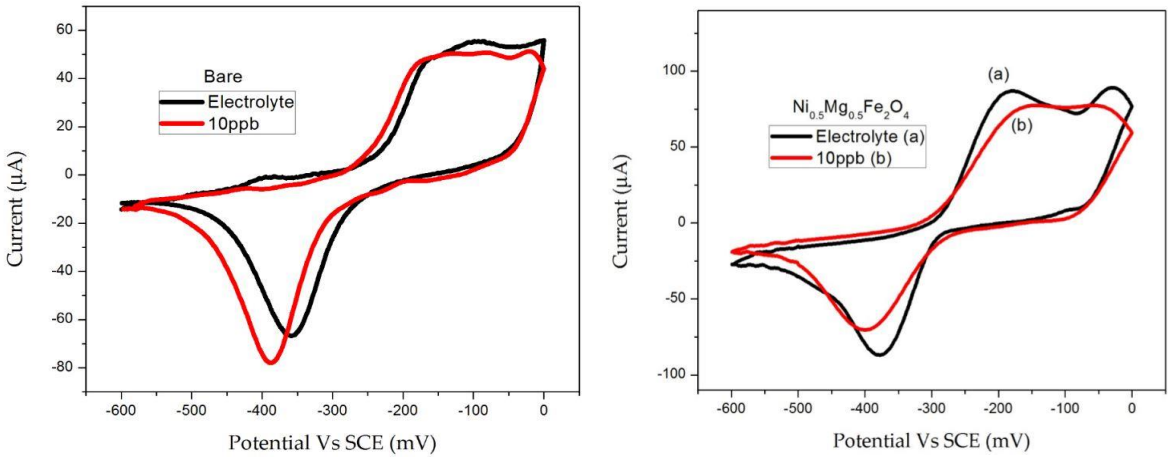

(a) (b)

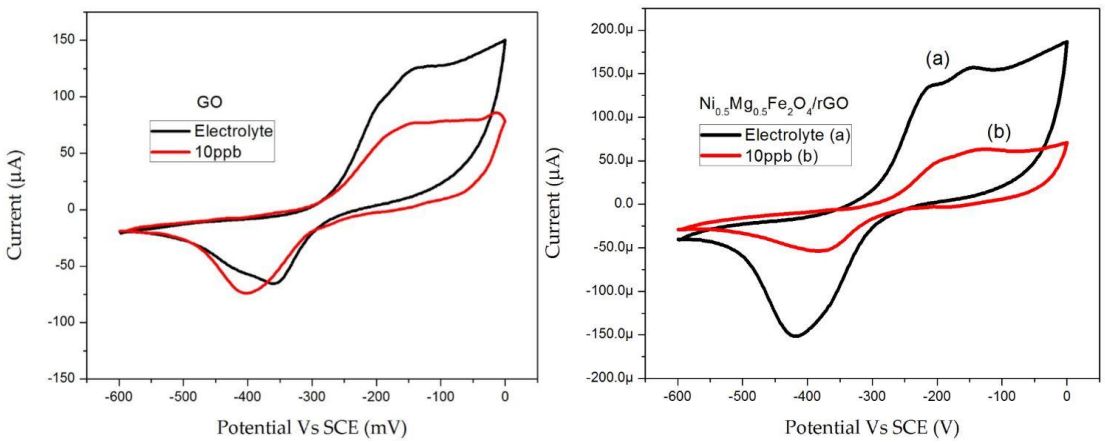

(c) (d)

Figure 3.9 Cyclic voltammogram of (a) bare, (b) $Ni_{0.5}Mg_{0.5}Fe_2O_4$, (c) GO, (d) $Ni_{0.5}Mg_{0.5}Fe_2O_4$/rGO in 10ppb lead containing 0.1M KOH

Figure 3.9 shows the CV responses of a bare interdigitated electrode and a modified interdigitated electrode includes Ni-Mg ferrites, reduced graphene oxide and GO/Ferrite composite. The graphs shows the detection of 10ppb lead ions (Pb^{2+}) in 0.1M KOH. Figure 3.9 (a) shows no detection of Pb by bare electrode, as the graph shows no change and approximately similar current was observed. Similarly figure 3.9 (b) also not shows any pronounce change in the graph before and after detection of lead. Figure 3.9 (c) and 3.9 (d) shows major changes in graph before and after detection of lead. It clearly shows the decreased peak of cathodic and anodic currents. It is also shown that a maximum detection is shown by Ni-Mg/ferrite composite.

IDE	I (µA) (Before Lead)	I (µA) (After 10ppb Lead)	Charge (µC) (Before Lead)	Charge µ(C) (After 10ppb Lead)
Bare	51.07	50.13	79.86	89.21
$Ni_{0.5}Mg_{0.5}Fe_2O_4$	94.04	91.06	162.4	
GO	150.5	85.96	260.3	153.6
$Ni_{0.5}Mg_{0.5}Fe_2O_4$/rGO	186.8	70.73	350.7	104.8

Table 3.2 Current and charge before and after detection of 10ppb lead

Table 3.2 shows the current and charge before and after detection of lead in 0.1M KOH. The bare and $Ni_{0.5}Mg_{0.5}Fe_2O_4$ modified IDE does not show any significant change in current, while in case of GO and Ferrite/rGO composite a significant change in current was observed. This shows that a much higher detection was obtained by using Ferrite/rGO composite. The charge also decreases before and after detection of lead.

3.4.3 Detection of 20ppb lead using modified interdigitated electrode

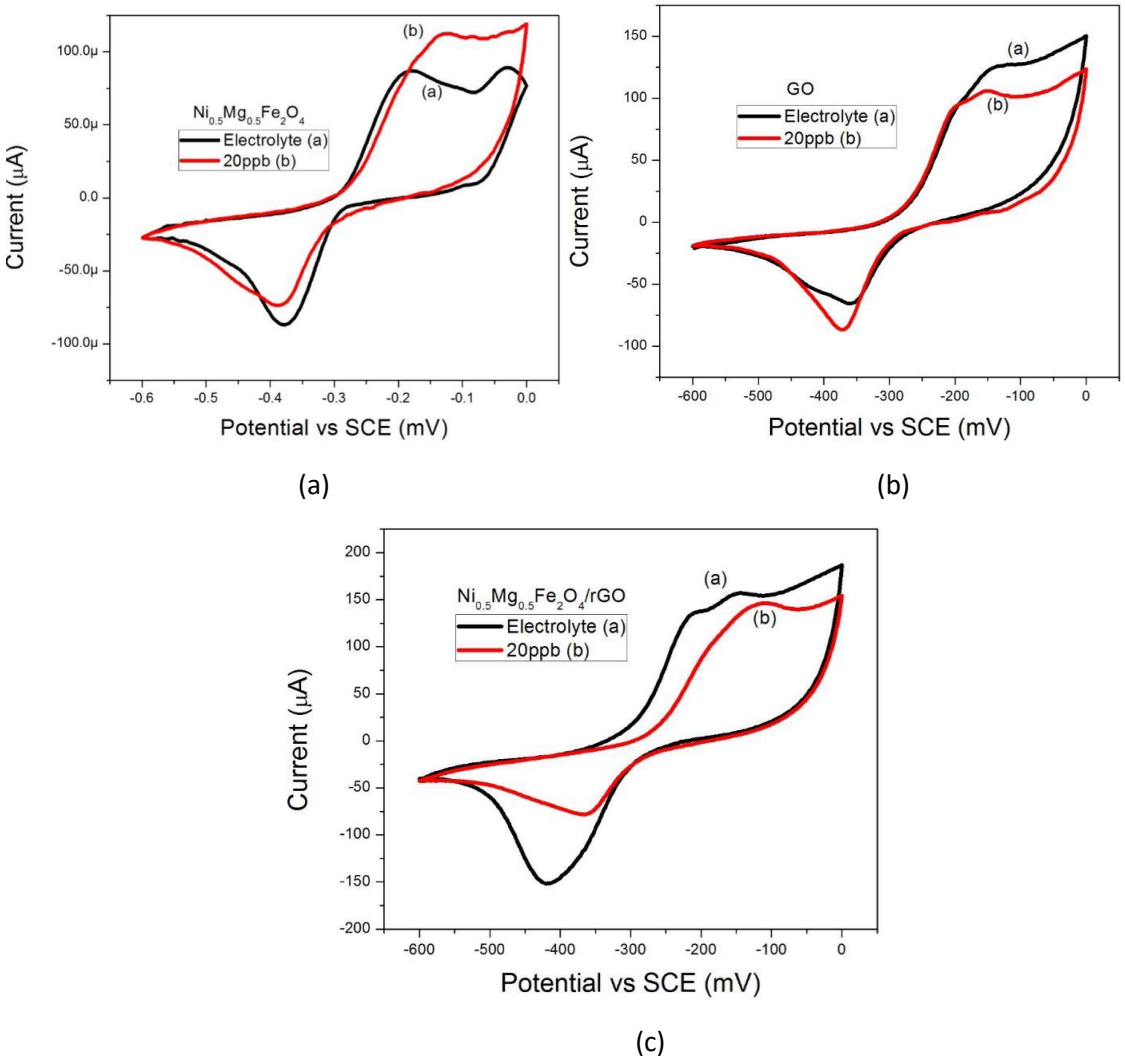

Figure 3.10 Cyclic voltammogram of (a) $Ni_{0.5}Mg_{0.5}Fe_2O_4$, (b) GO and (c) $Ni_{0.5}Mg_{0.5}Fe_2O_4$/rGO in 20ppb lead containing 0.1M KOH

CV responses of the modified IDEs were used for the detection of 20ppb lead in 0.1M KOH (Figure 3.10). A very slight detection of lead by Ni-Mg ferrites is shown in figure 3.10 (a) and a considerable detection is shown when these ferrites are combined with reduced graphene oxide as shown in figure 3.10 (c). As described earlier this is due

to the enhanced electronic pathway when we use Ni-Mg ferrites with reduced graphene oxide. While in case of ferrite modified IDE it may attributes to the oxide ions present of the surface of the IDE which hinders the transportation of electrons. In case of GO, detection is also shown in figure 3.10 (b). As seen from the previous graphs, by increasing the concentration of Pb ions the detection is also increased.

Bare	I (µA) (Before Lead)	I (µA) (After 20ppb Lead)	Charge (µC) (Before Lead)	Charge µ(C) (After 20ppb Lead)
$Ni_{0.5}Mg_{0.5}Fe_2O_4$	94.04	119.3	162.4	205.7
GO	150.5	123.7	260.3	225.1
$Ni_{0.5}Mg_{0.5}Fe_2O_4$/rGO	186.8	154.4	350.7	242

Table 3.3 Current and charge before and after detection of 20ppb lead

Table 3.3 shows the peak current and charge before and after detection of 20ppb lead. As we compare this from 10ppb lead detection the current increases as we increase the concentration of lead. This shows that more number of electrons are present that can interact at the electrode surface resulting in the enhancement of the signal generated.

3.4.4 Detection of 50ppb lead using GO and $Ni_{0.5}Mg_{0.5}Fe2O4$/rGO modified interdigitated electrode

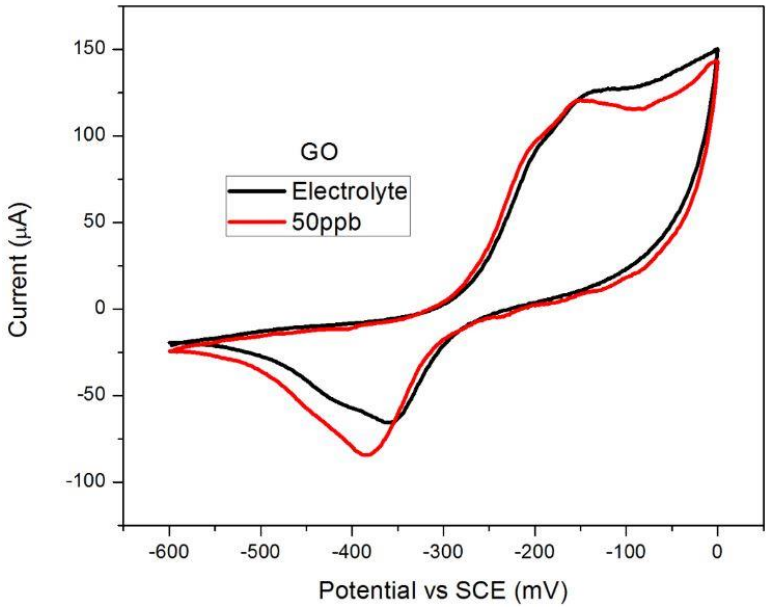

(a)

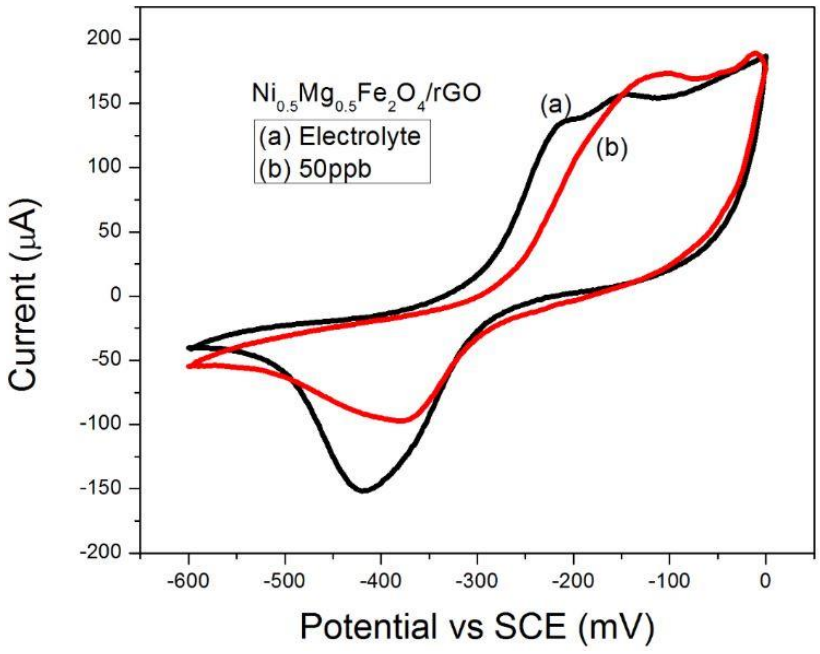

(b)

Figure 3.11 Cyclic voltammogram of (a) GO and (b) $Ni_{0.5}Mg_{0.5}Fe_2O_4$/rGO in 50ppb lead containing 0.1M KOH

IDE	I (μA) (Before Lead)	I (μA) (After 50ppb Lead)	Charge (μC) (Before Lead)	Charge μ(C) (After 50ppb Lead)
GO	150.5	143.5	260.3	246.9
$Ni_{0.5}Mg_{0.5}Fe_2O_4$/rGO	186.8	189.2	350.7	290.3

Table 3.4 Peak current and charge before and after detection of 50ppb lead

Table 3.4 shows the peak current and charge before and after detection of 50ppb lead. As we compare this from 10ppb and 20ppb lead detection the current increases as we increase the concentration of lead. This shows that more number of electrons can interact at the electrode surface resulting in the enhancement of the signal generated (Figure 3.11).

3.4.5 Detection of 100ppb and 500ppb lead using $Ni_{0.5}Mg_{0.5}Fe_2O_4$/rGO modified interdigitated electrode

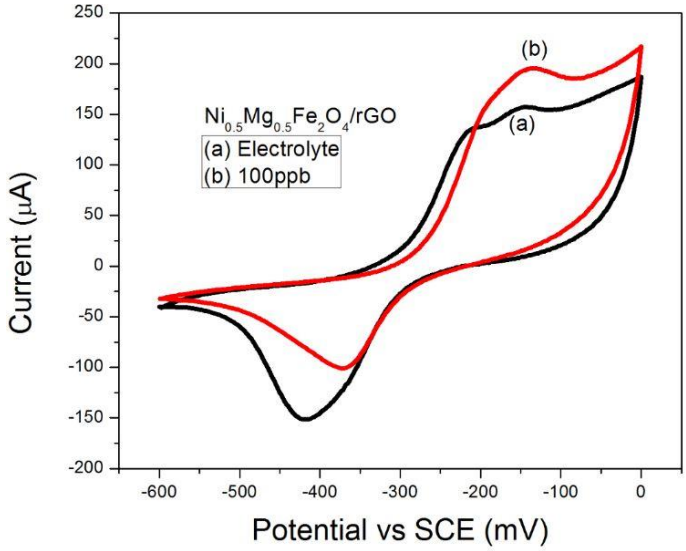

Figure 3.12 Cyclic voltammogram of $Ni_{0.5}Mg_{0.5}Fe_2O_4$/rGO in 100ppb containing 0.1M KOH

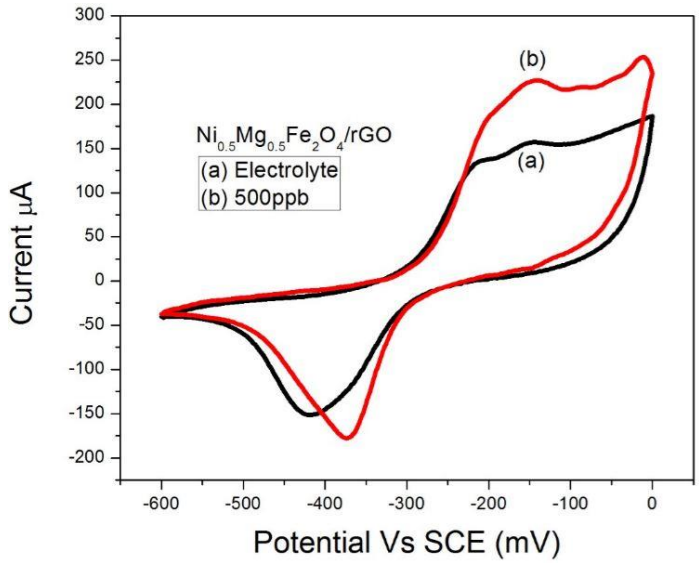

Figure 3.13 Cyclic voltammogram of $Ni_{0.5}Mg_{0.5}Fe_2O_4$/rGO in 500ppb containing 0.1M KOH

$Ni_{0.5}Mg_{0.5}Fe_2O_4$/rGO	I (μA) (Before Lead)	I (μA) (After Lead)	Charge (μC) (Before Lead)	Charge μ(C) (After Lead)
100ppb	186.8	216.8	350.7	387.1
500ppb	186.8	253.7	350.7	489.7

Table 3.5 Peak current before and after detection of 50ppb and 100ppb lead

3.4.6 Calibration curve of different concentrations of lead

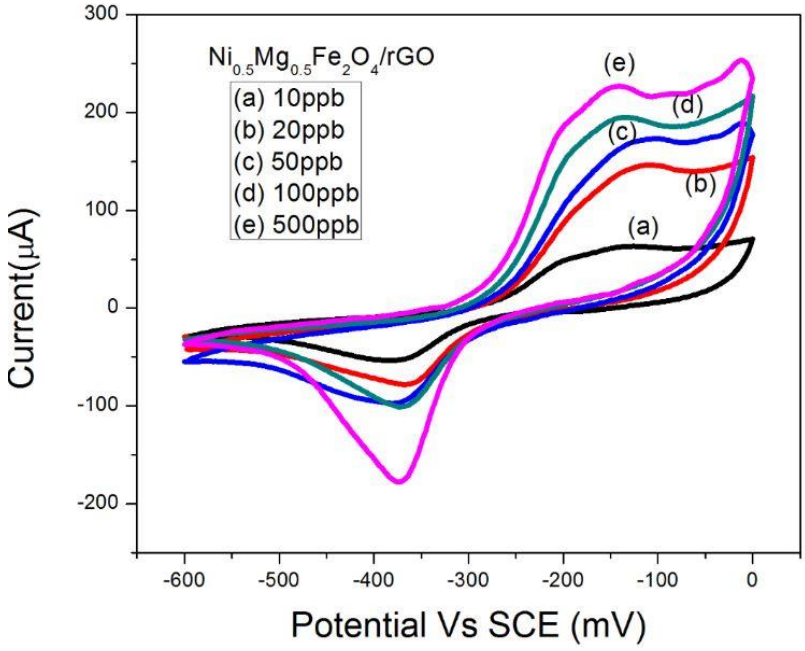

(a)

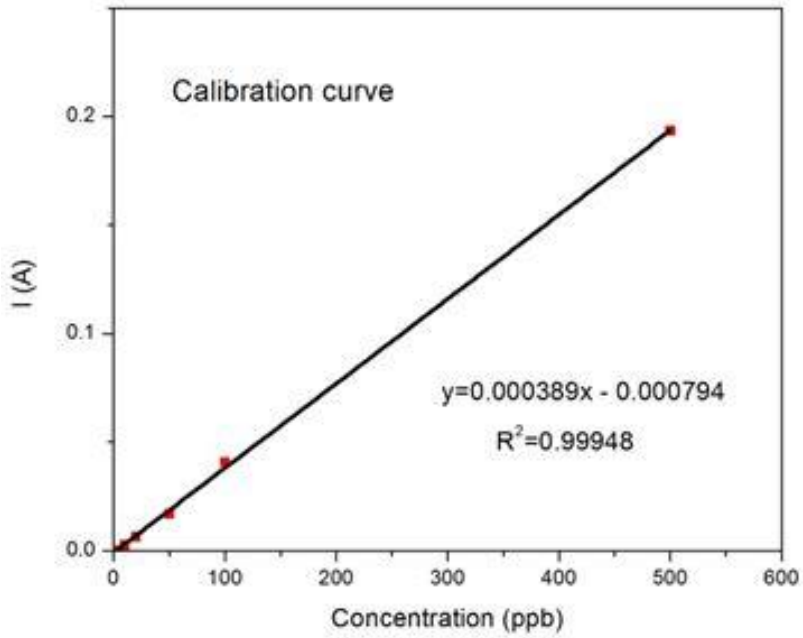

(b)

Figure 3.14 (a) Cyclic voltammograms of 10-500ppb concentrations of lead (b) Calibration curve of the $Ni_{0.5}Mg_{0.5}Fe_2O_4$/rGO modified IDE over a concentration range from 10-500ppb

Calibration curve is used to find the limit of detection (LOD) and sensivity of a sensor. Figure 3.14b shows the calibration plot of the Ni-Mg/ferrite composite modified IDE over a concentration range from 10-500ppb (Figure 3.14a). The linearization equation was found to be y=0.000389x-0.000794, and the correlation coefficient of 0.99948.

Calculating Limit of Detection (LOD):

LOD was calculated using 3Ʊ method.

$$LOD = \frac{3.3 * \text{standard deviation}}{\text{Slope}}$$

	Value	Standard Error
Intercept	-7.93996E-4	8.32357E-4
Slope	3.89045E-4	3.97564E-6

Table 3.6 parameters of the calibration curve

Table 3.6 shows the parameters of the calibration curve calculated using analysis tool in the origin software. LOD was found to be 7.06 ppb.

The slope of the calibration curve (current vs. concentration) gives the sensitivity of the sensor, which in this case is 0.000389 A ppb^{-1}.

3.5 Electrochemical Impedance spectroscopy (EIS)

3.5.1 Electrochemical characterization of Bare and modified IDE in 0.1M KOH

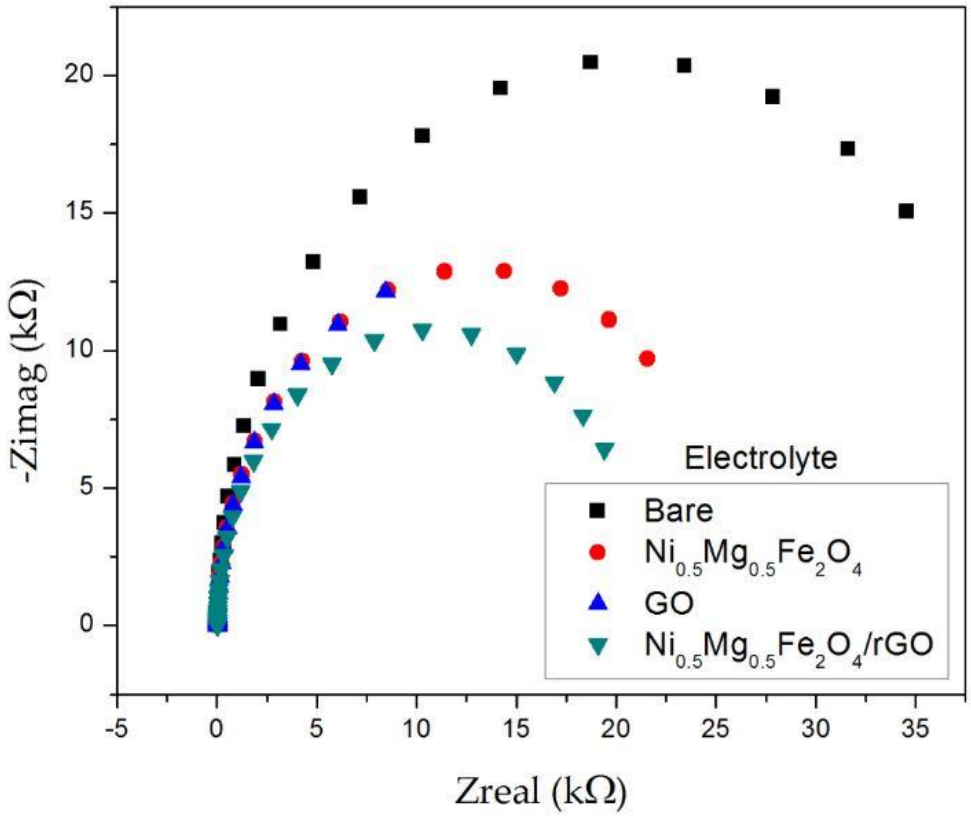

Figure 3.15 Fitted EIS responses of bare and modified IDE in 0.1M electrolyte

Figure 3.15 shows the fitted Nyquist EIS response of bare and modified IDE in 0.1M KOH. The figure shows the contribution from the kinetics of the reaction, no mass diffusion was observed. The plots shows the charge transfer resistance (R_{ct}) of bare (41.08kΩ), $Ni_{0.5}Mg_{0.5}Fe_2O_4$ (25.93kΩ), GO (25.85kΩ) and $Ni_{0.5}Mg_{0.5}Fe_2O_4$/rGO (25.50kΩ), is calculated using Echem analyst software. Charge transfer resistance showed that by depositing the sensing films on the interdigitated electrode the R_{ct} decreases because of the increase in current. This is attributed to the large surface area and increased adsorption capability of ferrites and excellent electrical conductivity of graphene and graphene oxide. The solution resistance (R_s) and capacitance (C) of bare (39.77Ω) (10.62μF), $Ni_{0.5}Mg_{0.5}Fe_2O_4$ (9.212Ω) (13.82μF), GO (25.18Ω) (4.442μF) and $Ni_{0.5}Mg_{0.5}Fe_2O_4$/rGO (15.90Ω) (12.26μF) is calculated respectively. The R_{ct} shows that these results are consistent with the CV results as shown in (Figure 3.8).

3.5.2 EIS response of $Ni_{0.5}MgFe_2O_4$ modified IDE in 10ppb and 20ppb lead

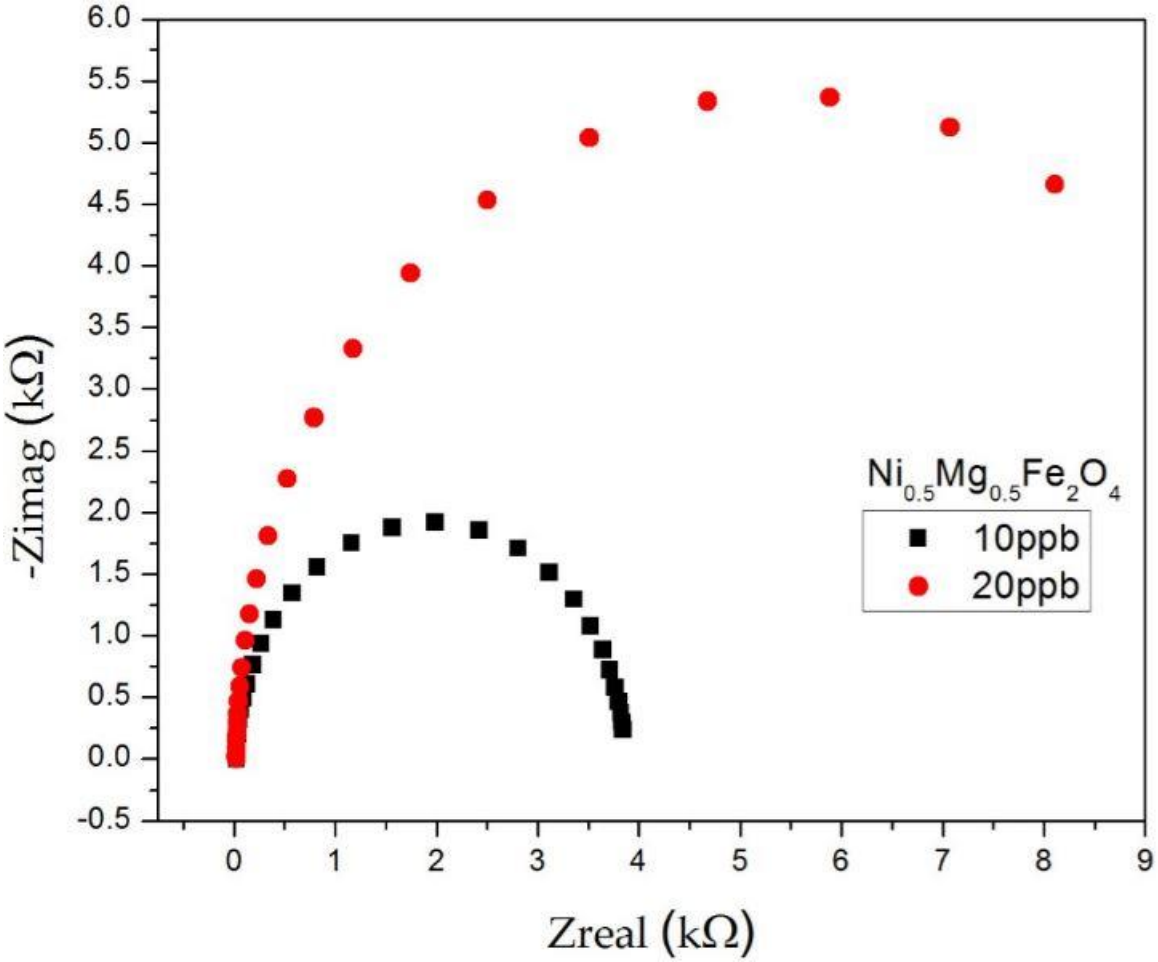

Figure 3.16 EIS responses of $Ni_{0.5}Mg_{0.5}Fe_2O_4$ modified IDE in 10ppb and 20ppb lead containing 0.1M KOH electrolyte

Figure 3.16 shows EIS response of the $Ni_{0.5}Mg_{0.5}Fe_2O_4$ modified IDE in 10ppb and 20ppb lead containing 0.1M KOH. The R_{ct} of 10ppb is 3.829kΩ and R_{ct} of 20ppb is 10.77kΩ. By increasing the concentration of lead, the charge transfer resistance increases due to the increase in current. Deposition of ferrites sensing film on the surface of IDEs increases the surface area of IDEs. These results have been found consistent with the CV results discussed earlier. The R_s of 10ppb and 20ppb is 30.13Ω and 26.45Ω.

3.5.3 EIS response of GO modified IDE in 10ppb, 20ppb and 50ppb lead

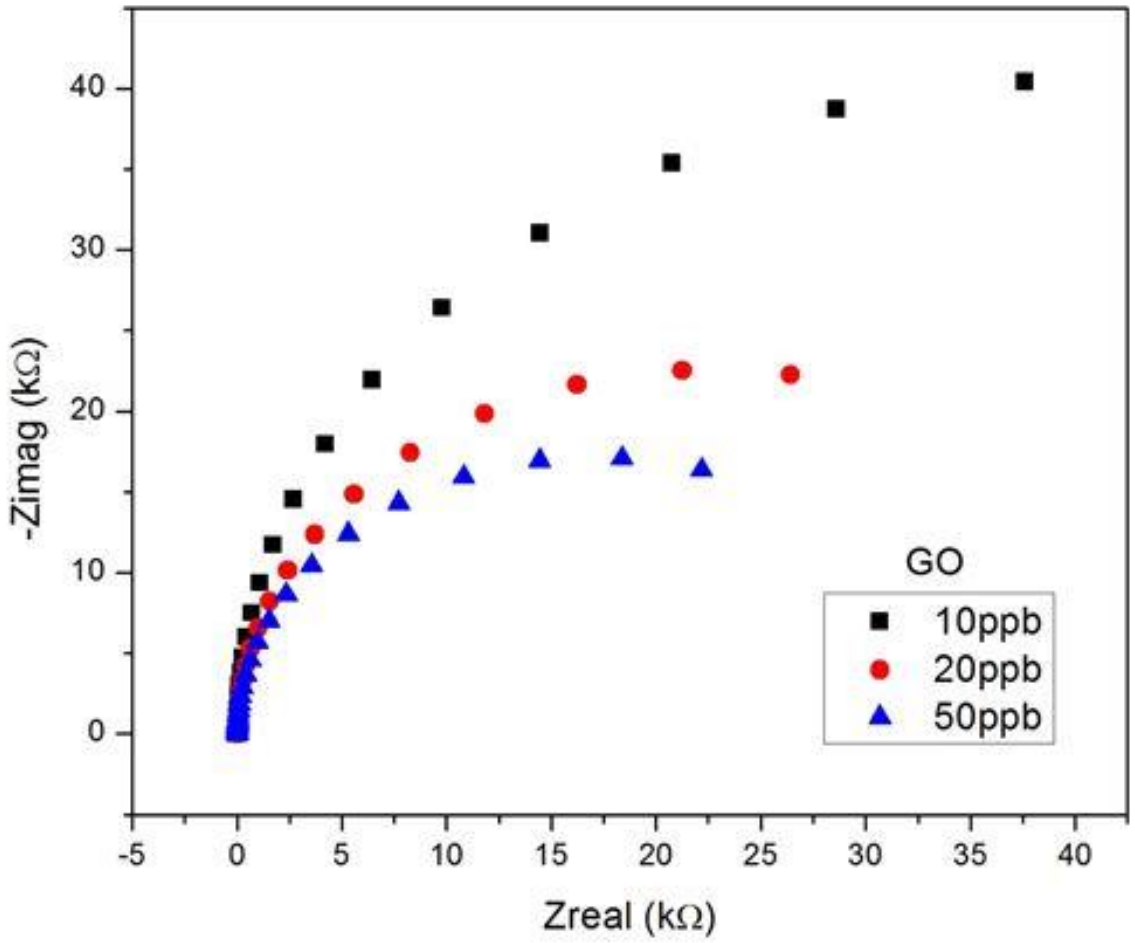

Figure 3.17 EIS response of GO modified IDE in 10ppb, 20ppb and 50ppb lead containing 0.1M KOH

Figure 3.17 shows the fitted EIS plots of GO modified IDE in different concentrations ranging from 10ppb-50ppb. The graph shows that as we increase the concentration of lead, the charge transfer resistance decreases as the current increases. This is because GO has an excellent electrical conductivity which enhances the transfer of electrons at the surface of the IDE. These results have been found consistent with the CV results discussed earlier. The values of the R_{ct}, R_s and C can be found from table 3.7, 3.8 and 3.9, respectively.

3.5.4 EIS response of $Ni_{0.5}Mg_{0.5}Fe_2O_4$/rGO modified IDE in different concentration of lead

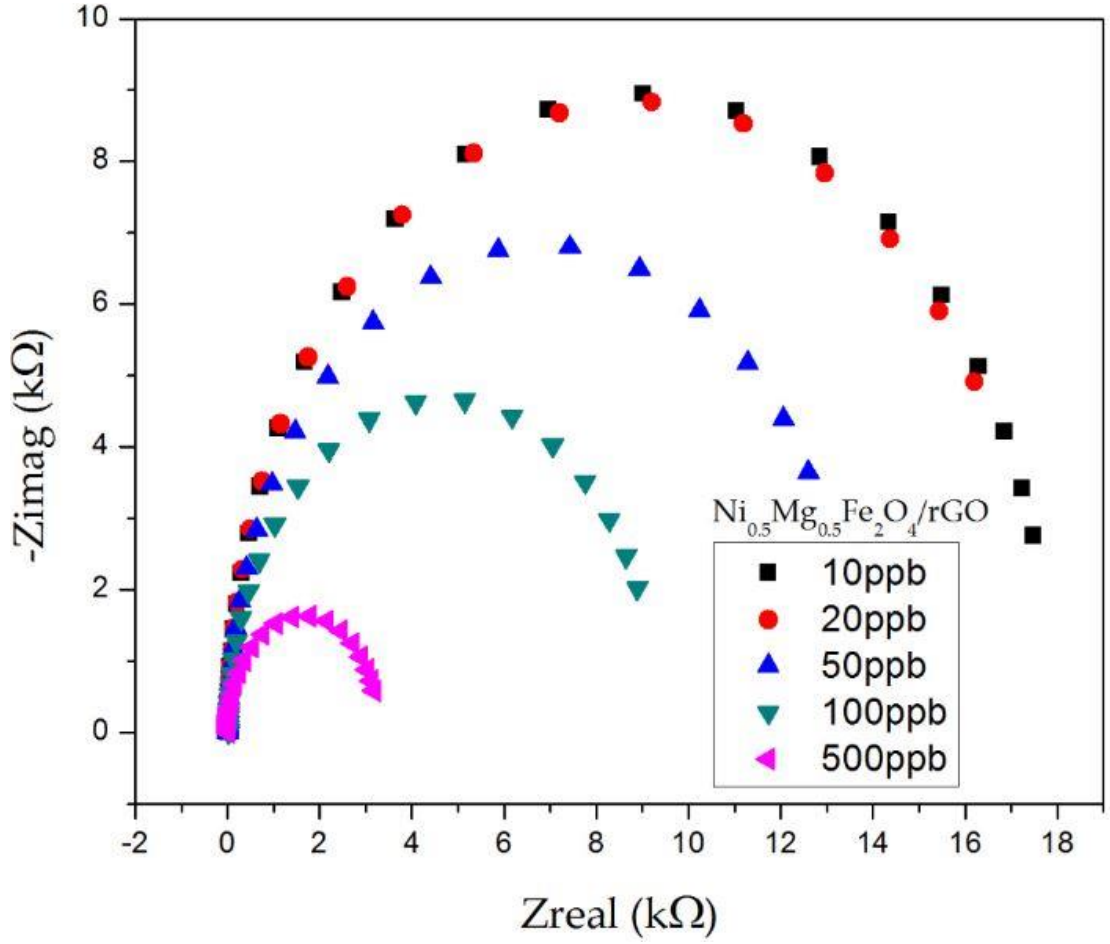

Figure 3.18 EIS response of $Ni_{0.5}Mg_{0.5}Fe_2O_4$/rGO modified IDE in different concentration of lead containing 0.1M KOH

Fitted EIS plots (figure 3.18) of different concentrations of lead show that as we increase the concentration of lead ranging from 10ppb-500ppb the charge transfer resistance decreases, as the current increases shown in figure 3.14a. By increasing the concentration more electrons can flow at the surface of IDE. By depositing $Ni_{0.5}Mg_{0.5}Fe_2O_4$/rGO film not only enhances the transport of electrons at the surface of the IDEs but also increases the surface area of the IDEs. The enhanced transport of electrons is attributed to the excellent electrical properties of reduced graphene oxide. The values of R_{ct}, R_s and C can be found from table 3.7, 3.8 and 3.9 respectively.

	Bare	$Ni_{0.5}Mg_{0.5}Fe_2O_4$	GO	$Ni_{0.5}Mg_{0.5}Fe_2O_4$/rGO
Electrolyte	41.08	25.93	25.85	21.50
10ppb	-	3.829	80.97	17.89
20ppb	-	10.77	45.15	17.68
50ppb	-	-	34.23	13.64
100ppb	-	-	-	9.334
500ppb	-	-	-	3.27

Table 3.7 Charge transfer resistane (R_{ct}) of bare and modified IDEs in different concentrations of lead

	Bare	$Ni_{0.5}Mg_{0.5}Fe_2O_4$	GO	$Ni_{0.5}Mg_{0.5}Fe_2O_4$/rGO
Electrolyte	39.77	9.212	25.18	15.90
10ppb	-	14.55	15.45	23.37
20ppb	-	30.13	13.84	78.26
50ppb	-	-	23.71	14.76
100ppb	-	-	-	11.62
500ppb	-	-	-	19.28

Table 3.8 Solution resistance (R_s) of bare and modified IDEs in different concentrations of lead

	Bare	$Ni_{0.5}Mg_{0.5}Fe_2O_4$	GO	$Ni_{0.5}Mg_{0.5}Fe_2O_4$/rGO
Electrolyte	10.62	13.82	4.442	12.26
10ppb	-	12.81	10.59	7.030
20ppb	-	4.275	14.89	13.70
50ppb	-	-	17.21	16.94
100ppb	-	-	-	19.41
500ppb	-	-	-	44.89

Table 3.9 Capacitance (C) of bare and modified IDEs in different concentrations of lead

3.6 Linear Sweep Voltammetry (LSV)

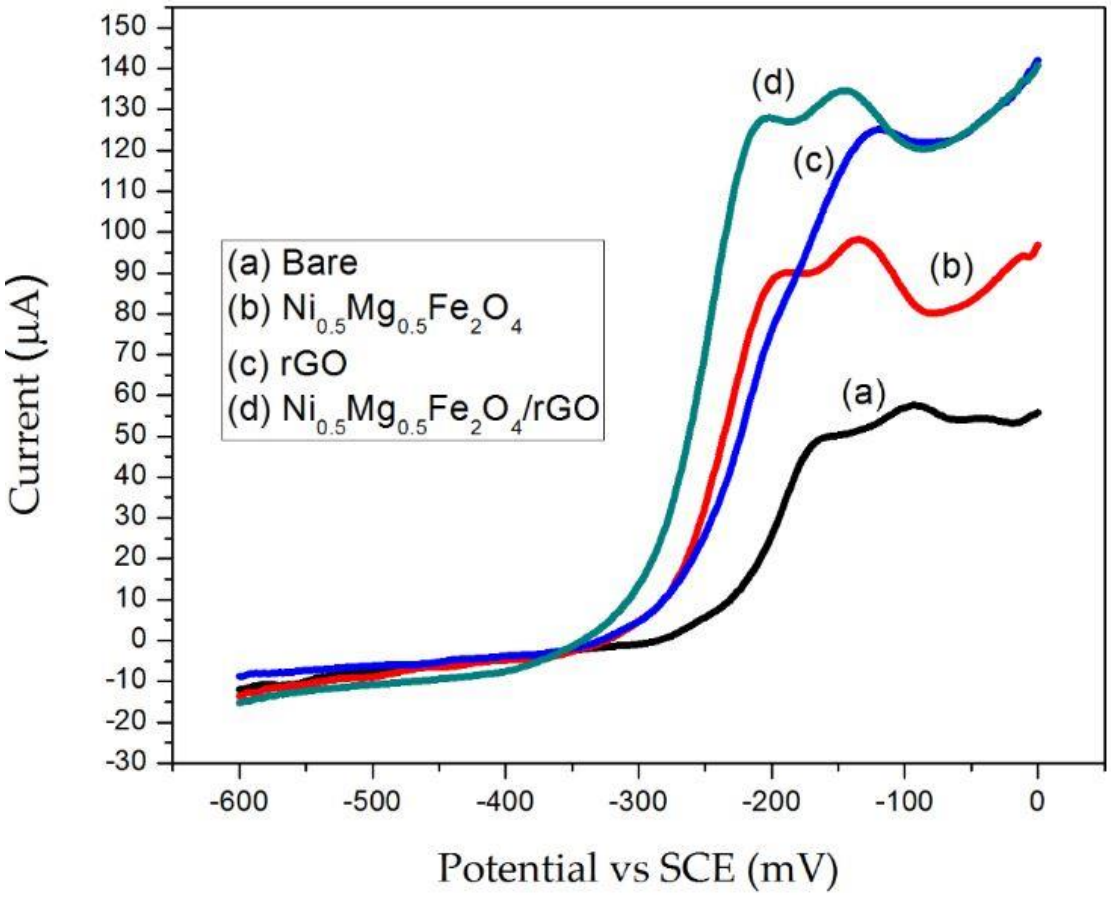

Figure 3.19 Linear sweep voltammetry of bare and modified IDE in 0.1M KOH

Figure 3.19 shows the LSV of bare and modified IDE in 0.1M KOH. The figure shows the maximum current by $Ni_{0.5}Mg_{0.5}Fe_2O_4$/rGO and a minimum current by bare IDE, which are also consistent with the CV results as shown in Figure 3.8. These results shows that maximum detection is possible with $Ni_{0.5}Mg_{0.5}Fe_2O_4$/rGO as more transportation of electrons occurs at the surface of the $Ni_{0.5}Mg_{0.5}Fe_2O_4$/rGO modified IDE.

3.6.1 Detection of 10ppb lead using bare and modified interdigitated electrode

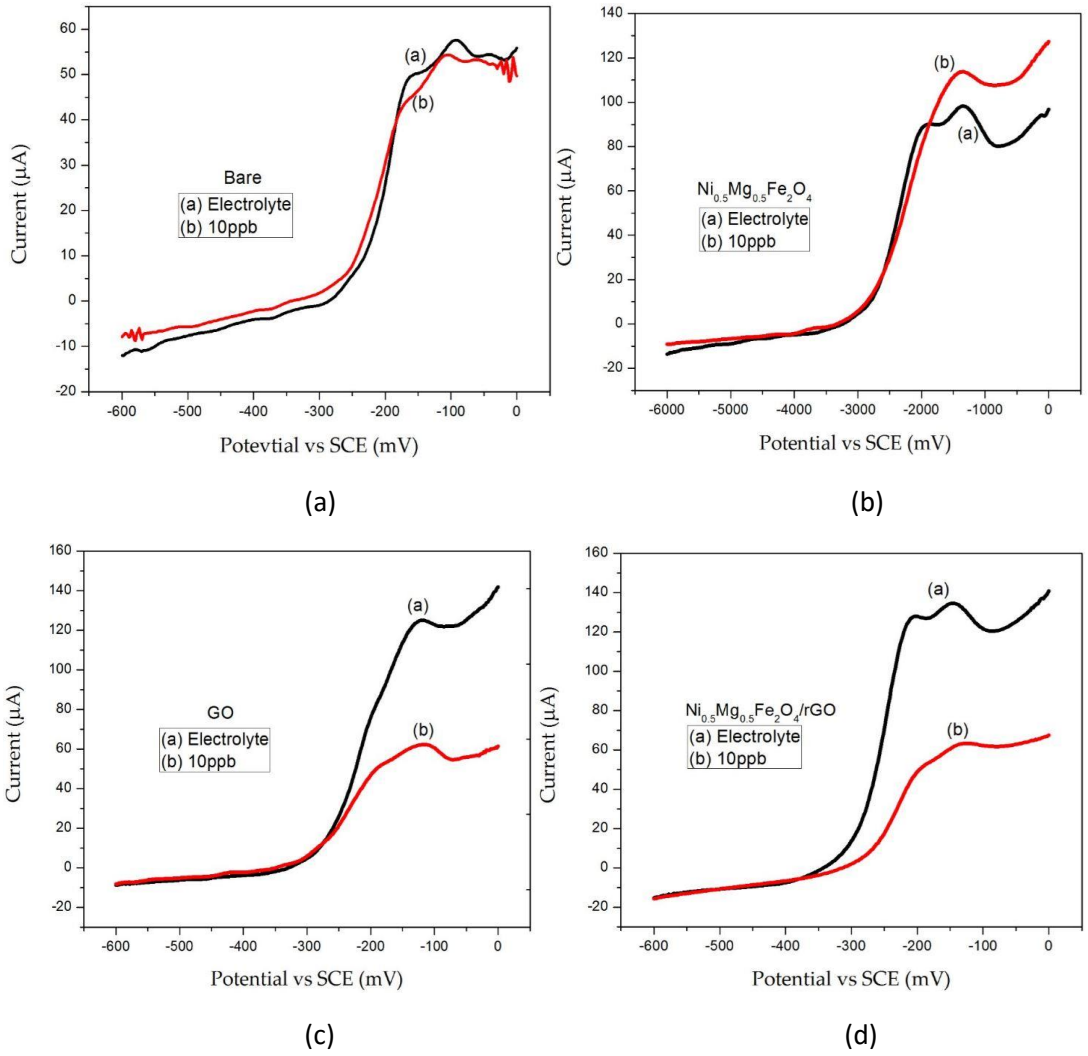

Figure 3.20 LSV of (a) bare, (b) $Ni_{0.5}Mg_{0.5}Fe_2O_4$, (c) GO and (d) $Ni_{0.5}Mg_{0.5}Fe_2O_4$/rGO in 10ppb lead containing 0.1M KOH

Figure 3.20 (a) shows the detection of lead using bare IDE and no detection of lead is observed in case of bare IDE. $Ni_{0.5}Mg_{0.5}Fe_2O_4$ modified IDE show a little detection as the graph does not show a pronounce change as shown in figure 3.20 (b). GO and $Ni_{0.5}Mg_{0.5}Fe_2O_4$/rGO modified IDE showed the detection of lead as the current decreases compared from their characterization in electrolyte. These results are also consistent with results obtained from cyclic voltammograms as shown in Figure 3.9.

3.6.2 Detection of 20ppb lead using modified interdigitated electrode

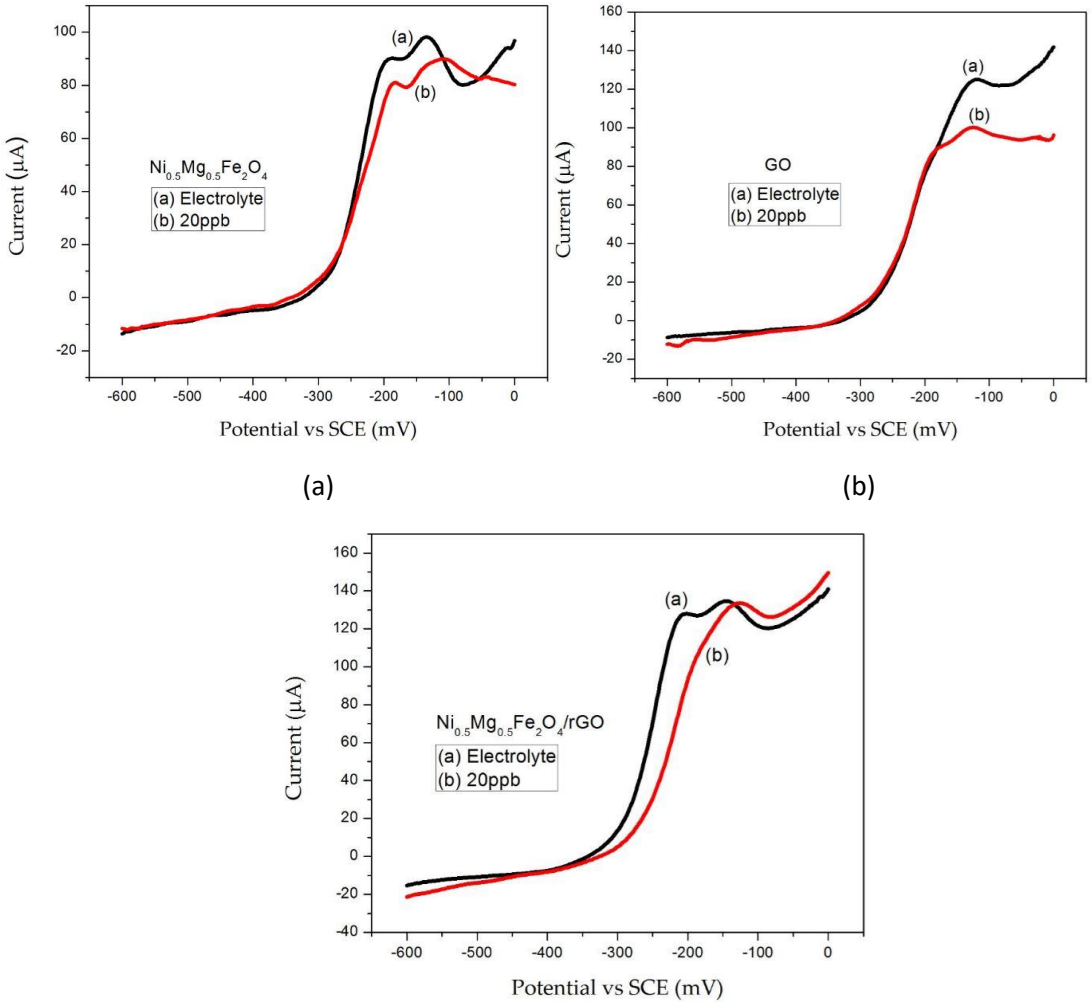

Figure 3.21 LSV of (a) $Ni_{0.5}Mg_{0.5}Fe_2O_4$, (b) GO and (c) $Ni_{0.5}Mg_{0.5}Fe_2O_4$/rGO in 20ppb containing 0.1M KOH

By increasing the concentration of lead the current increases as shown in figure 3.21. The current increases more in case of $Ni_{0.5}Mg_{0.5}Fe_2O_4$/rGO as compared to GO. The current increases both in figure 3.21 (b) and (c) because GO has much higher conductivity and this is attributed to the structure of the GO but due to the presence of magnetic nanoparticles with rGO the current is enhanced due to increased surface area and presence of more oxide groups on the surface of $Ni_{0.5}Mg_{0.5}Fe_2O_4$/rGO IDE.

3.6.3 Detection of 50ppb lead using modified interdigitated electrode

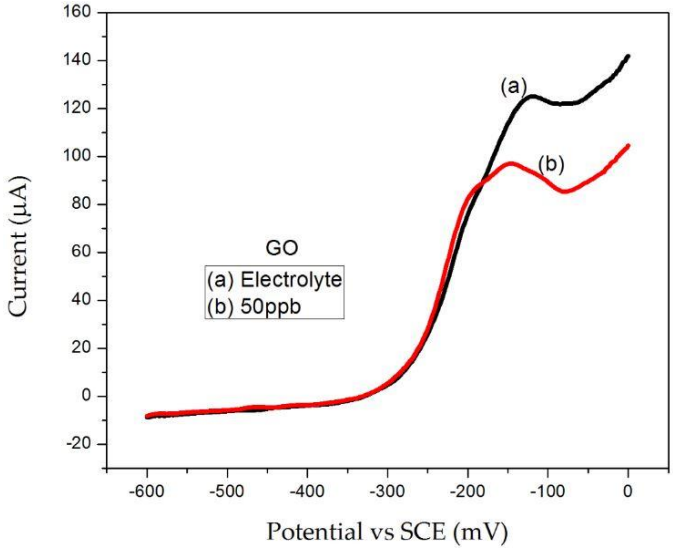

(a)

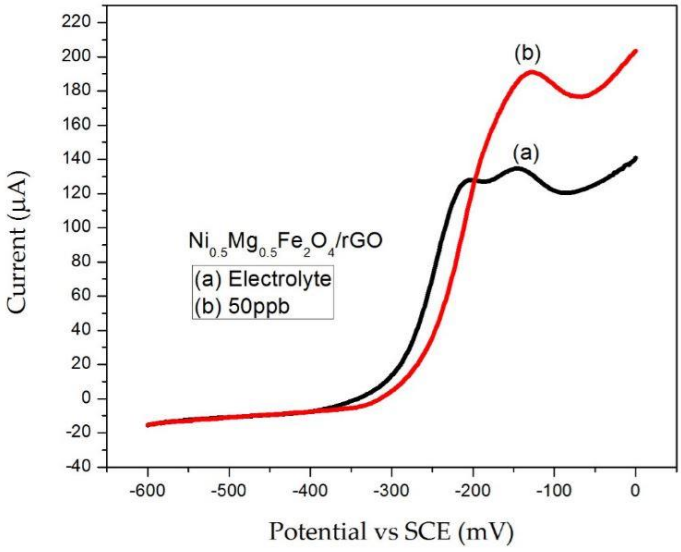

(b)

Figure 3.22 LSV of (a) GO and (b) $Ni_{0.5}Mg_{0.5}Fe_2O_4$/rGO modified IDE in 50ppb containing 0.1M KOH

Linear sweep voltammograms of GO and $Ni_{0.5}Mg_{0.5}Fe_2O_4$/rGO modified IDEs in 50ppb lead containing 0.1MKOH were shown in figure 3.22. The graphs show that an increase detection is observed in case of $Ni_{0.5}Mg_{0.5}Fe_2O_4$/rGO nanocomposite. By increasing the concentration more electrons are present at the surface of IDEs. By the

addition of ferrites to rGO the surface area also increases which shows the enhancement in the conductivity.

3.6.4 Detection of 100ppb and 500ppb lead using modified interdigitated electrode

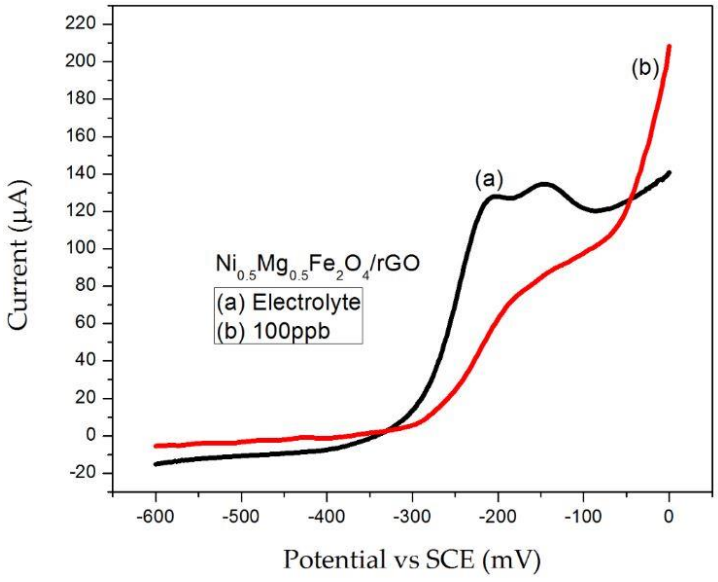

(a)

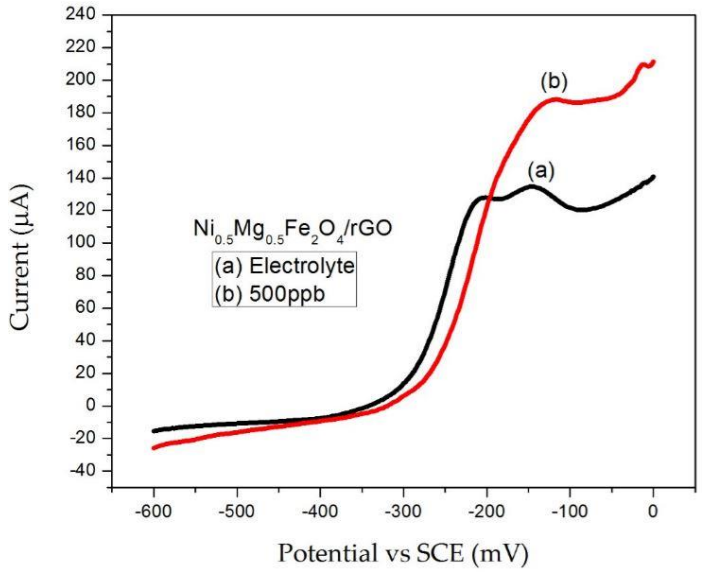

(b)

Figure 3.23 LSV of $Ni_{0.5}Mg_{0.5}Fe_2O_4$/rGO IDE (a) 100ppb and (b) 500ppb lead in 0.1M KOH

3.6.5 Lead concentration ranging from 10ppb-500ppb in 0.1M KOH

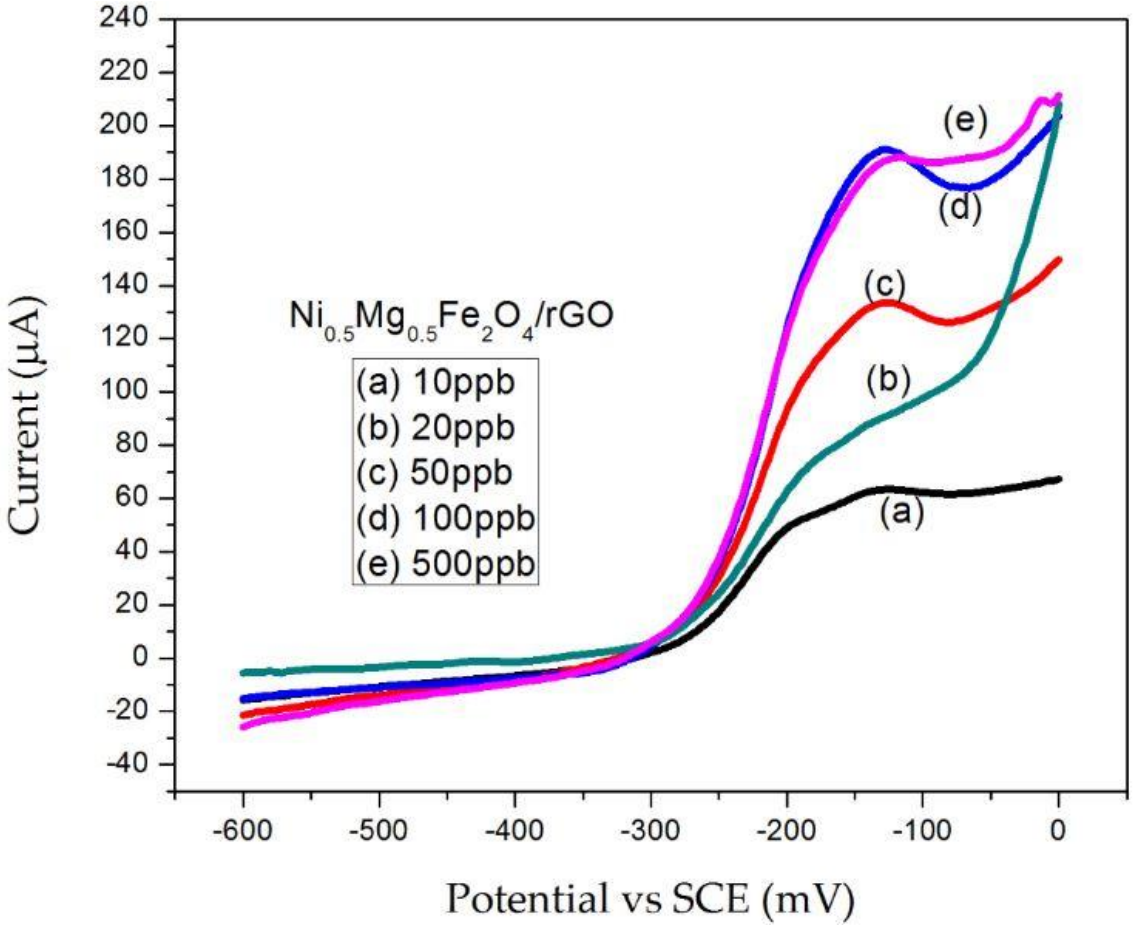

Figure 3.24 LSV of different concentrations of Pb ranging from 10ppb to 500ppb

Figure 3.24 shows the Linear sweep voltammograms of $Ni_{0.5}Mg_{0.5}Fe_2O_4$/rGO modified IDE in different concentrations of lead (10ppb, 20ppb, 50ppb, 100ppb and 500ppb). The plots shows that by increasing the concentration of lead, current increases. This is due to the increased number of electrons present at the surface of IDE. Details were already explained in section 3.4.

Chapter 4
Conclusions

In this research work, electrochemical response of interdigitated electrodes modified with sensing materials $Ni_{0.5}Mg_{0.5}Fe_2O_4$ ferrites, graphene oxide and $Ni_{0.5}Mg_{0.5}Fe_2O_4$/rGO towards Pb^{2+} ions was studied. It was observed that the $Ni_{0.5}Mg_{0.5}Fe_2O_4$/rGO nanocomposite showed the best response towards Pb^{2+} ions.

Copper based IDEs were successfully fabricated by using a simple, fast and low cost method that involved fewer processing steps and cheap investment. The sensing materials were synthesized and successfully characterized by SEM and XRD techniques. The average particle size obtained was 20 nm and XRD graphs reveal that all the peaks obtained show successful synthesis of sensing materials.

The electrochemical sensor was fabricated by depositing thin films of sensing materials on IDEs. These modified IDEs were used as working electrode in the three electrode system of a potentiostat. Electrochemical techniques such as LSV, CV and EIS were performed on these modified IDEs in 0.1M KOH electrolytic solution and their electrochemical response towards Pb^{2+} ions were observed.

It was concluded that among the three sensing materials used, $Ni_{0.5}Mg_{0.5}Fe_2O_4$/rGO nanocomposite modified IDEs has higher sensitivity towards Pb^{2+} ions. The sensitivity achieved by using $Ni_{0.5}Mg_{0.5}Fe_2O_4$/rGO nanocomposite as a sensing element is 0.000389 $\mu A\ ppb^{-1}$ and limit of detection (LOD) obtained is 7.06 ppb.

References

[1] M.B. Gumpu, S. Sethuraman, U.M. Krishnan, J.B.B. Rayappan, A review on detection of heavy metal ions in water–An electrochemical approach, Sensors and Actuators B: Chemical, 213**(2015)** 515-33.

[2] S.K. Agarwal, Heavy Metal Pollution, New Delhi: S.B. Nangia; **(2009)**.

[3] G.L. Turdean, Design and development of biosensors for the detection of heavy metal toxicity, International Journal of Electrochemistry, 2011**(2011)**.

[4] A. Singh, R.K. Sharma, M. Agrawal, F.M. Marshall, Health risk assessment of heavy metals via dietary intake of foodstuffs from the wastewater irrigated site of a dry tropical area of India, Food and Chemical Toxicology, 48**(2010)** 611-9.

[5] L.M. da Costa Silva, A.F. Melo, A.M. Salgado, Biosensors for Environmental Applications, Edited by Vernon Somerset, **(2011)** 1.

[6] G. Aragay, A. Merkoçi, Nanomaterials application in electrochemical detection of heavy metals, Electrochimica Acta, 84**(2012)** 49-61.

[7] J. Zhu, S. Wei, M. Chen, H. Gu, S.B. Rapole, S. Pallavkar, et al., Magnetic nanocomposites for environmental remediation **(2013)**.

[8] T. Zoumis, A. Schmidt, L. Grigorova, W. Calmano, Contaminants in sediments: remobilisation and demobilisation, Science of the total environment, 266**(2001)** 195-202.

[9] P. Quevauviller, G. Rauret, J.-F. Lopez-Sanchez, R. Rubio, A. Ure, H. Muntau, Certification of trace metal extractable contents in a sediment reference material (CRM 601) following a three-step sequential extraction procedure, Science of the Total Environment, 205**(1997)** 223-34.

[10] M. Arribere, S.R. Guevara, R. Sanchez, M. Gil, G.R. Ross, L. Daurade, et al., Heavy metals in the vicinity of a chlor-alkali factory in the upper Negro River ecosystem, Northern Patagonia, Argentina, Science of the total environment, 301**(2003)** 187-203.

[11] J. Li, Y. Lu, A highly sensitive and selective catalytic DNA biosensor for lead ions, Journal of the American Chemical Society, 122**(2000)** 10466-7.

[12] Y. Yang, Y. Zhang, J.-C. Shen, H. Yang, Z.-G. Zhou, S.-P. Yang, A highly selective magnetic sensor with functionalized Fe/Fe_3O_4 nanoparticles for detection of Pb^{2+}, Chinese Chemical Letters, 27**(2016)** 891-5.

[13] Y. Finkelstein, M.E. Markowitz, J.F. Rosen, Low-level lead-induced neurotoxicity in children: an update on central nervous system effects, Brain Research Reviews, 27**(1998)** 168-76.

[14] F. Zahir, S.J. Rizwi, S.K. Haq, R.H. Khan, Low dose mercury toxicity and human health, Environmental toxicology and pharmacology, 20**(2005)** 351-60.

[15] D. Martín-Yerga, M.B. González-García, A. Costa-García, Electrochemical determination of mercury: a review, Talanta, 116**(2013)** 1091-104.

[16] G.K. Darbha, A.K. Singh, U.S. Rai, E. Yu, H. Yu, P. Chandra Ray, Selective detection of mercury (II) ion using nonlinear optical properties of gold nanoparticles, Journal of the American Chemical Society, 130**(2008)** 8038-43.

[17] N. Kongsricharoern, C. Polprasert, Electrochemical precipitation of chromium (Cr^{6+}) from an electroplating wastewater, Water Science and Technology, 31**(1995)** 109-17.

[18] K. Kadirvelu, K. Thamaraiselvi, C. Namasivayam, Removal of heavy metals from industrial wastewaters by adsorption onto activated carbon prepared from an agricultural solid waste, Bioresource technology, 76**(2001)** 63-5.

[19] W. Yantasee, Y. Lin, K. Hongsirikarn, G.E. Fryxell, R. Addleman, C. Timchalk, Electrochemical sensors for the detection of lead and other toxic heavy metals: the next generation of personal exposure biomonitors, Environmental Health Perspectives, **(2007)** 1683-90.

[20] Y. Kim, R.C. Johnson, J.T. Hupp, Gold nanoparticle-based sensing of "spectroscopically silent" heavy metal ions, Nano Letters, 1**(2001)** 165-7.

[21] J.-f. Peng, Y.-h. Song, P. Yuan, X.-y. Cui, G.-l. Qiu, The remediation of heavy metals contaminated sediment, Journal of hazardous materials, 161**(2009)** 633-40.

[22] M. Kumari, C.U. Pittman, D. Mohan, Heavy metals [chromium (VI) and lead (II)] removal from water using mesoporous magnetite (Fe_3O_4) nanospheres, Journal of colloid and interface science, 442**(2015)** 120-32.

[23] D.S. Mathew, R.-S. Juang, An overview of the structure and magnetism of spinel ferrite nanoparticles and their synthesis in microemulsions, Chemical Engineering Journal, 129**(2007)** 51-65.

[24] R.C. Pullar, Hexagonal ferrites: a review of the synthesis, properties and applications of hexaferrite ceramics, Progress in Materials Science, 57**(2012)** 1191-334.

[25] N.A. Spaldin, Magnetic materials: fundamentals and applications: Cambridge University Press; **2010**.

[26] E.A. Boudreaux, L. Mulay, Theory and applications of molecular paramagnetism: Wiley New York; **1976**.

[27] J.L. Snoek, New developments in ferromagnetic materials: Elsevier Publishing Company; **1949**.

[28] S.-F. Zhou, X.-J. Han, H.-L. Fan, Q.-X. Zhang, Y.-Q. Liu, Electrochemical detection of As (III) through mesoporous $MnFe_2O_4$ nanocrystal clusters by square wave stripping voltammetry, Electrochimica Acta, 174**(2015)** 1160-6.

[29] N.F. Atta, A. Galal, H. Ekram, Graphene—A Platform for Sensor and Biosensor Applications, **(2015)**.

[30] M.J. Allen, V.C. Tung, R.B. Kaner, Honeycomb carbon: a review of graphene, Chemical reviews, 110**(2009)** 132-45.

[31] Y. Shao, J. Wang, H. Wu, J. Liu, I.A. Aksay, Y. Lin, Graphene based electrochemical sensors and biosensors: a review, Electroanalysis, 22**(2010)** 1027-36.

[32] D.R. Dreyer, S. Park, C.W. Bielawski, R.S. Ruoff, The chemistry of graphene oxide, Chemical Society Reviews, 39**(2010)** 228-40.

[33] Y. Zhu, S. Murali, W. Cai, X. Li, J.W. Suk, J.R. Potts, et al., Graphene and graphene oxide: synthesis, properties, and applications, Advanced materials, 22**(2010)** 3906-24.

[34] A.C. Neto, F. Guinea, N.M. Peres, K.S. Novoselov, A.K. Geim, The electronic properties of graphene, Reviews of modern physics, 81**(2009)** 109.

[35] K.I. Bolotin, K. Sikes, Z. Jiang, M. Klima, G. Fudenberg, J. Hone, et al., Ultrahigh electron mobility in suspended graphene, Solid State Communications, 146**(2008)** 351-5.

[36] I. Ovid'ko, Mechanical properties of graphene, Rev Adv Mater Sci, 34**(2013)** 1-11.

[37] L. Falkovsky, Optical properties of graphene, Journal of Physics: Conference Series, IOP Publishing2008, p. 01**2004**.

[38] P.M. Ajayan, L.S. Schadler, P.V. Braun, Nanocomposite science and technology: John Wiley & Sons; **2006**.

[39] S. Anandhan, S. Bandyopadhyay, Polymer nanocomposites: from synthesis to applications: INTECH Open Access Publisher; **2011**.

[40] W. Luther, Industrial application of nanomaterials: chances and risks technological analysis. Vdi technologiezentrum, Germany, **(2004)**.

[41] A. Evans, C. San Marchi, A. Mortensen, Metal Matrix Composites, Metal Matrix Composites in Industry, Springer**2003**, pp. 9-38.

[42] M. Sternitzke, Structural ceramic nanocomposites, Journal of the European Ceramic Society, 17**(1997)** 1061-82.

[43] A.S. Edelstein, R. Cammaratra, Nanomaterials: synthesis, properties and applications: CRC Press; **1998**.

[44] C.N.R. Rao, A. Müller, A.K. Cheetham, Nanomaterials chemistry: recent developments and new directions: John Wiley & Sons; **2007**.

[45] D. Zhao, H. Yang, R. Li, J. Ma, W. Feng, Fabrication of nickel ferrite–graphene nanocomposites and their photocatalytic properties, Materials Research Innovations, 18**(2014)** 519-23.

[46] E. Peng, E.S.G. Choo, P. Chandrasekharan, C.T. Yang, J. Ding, K.H. Chuang, et al., Synthesis of manganese ferrite/graphene oxide nanocomposites for biomedical applications, Small, 8**(2012)** 3620-30.

[47] Y. Xiao, X. Li, J. Zai, K. Wang, Y. Gong, B. Li, et al., $CoFe_2O_4$-graphene nanocomposites synthesized through an ultrasonic method with enhanced performances as anode materials for Li-ion batteries, Nano-Micro Letters, 6**(2014)** 307-15.

[48] T.A. Rocha-Santos, Sensors and biosensors based on magnetic nanoparticles, TrAC Trends in Analytical Chemistry, 62**(2014)** 28-36.

[49] N.F. Carter, G.R. Chambers, G.J. Hughes, S. Scott, G.S. Sanghera, J.L. Watkin, Electrochemical sensor, Google Patents**1997**.

[50] I. Oehme, O.S. Wolfbeis, Optical sensors for determination of heavy metal ions, Microchimica Acta, 126**(1997)** 177-92.

[51] D.-I.E.G. Gautschi, Piezoelectric sensors, Piezoelectric Sensorics, Springer**2002**, pp. 73-91.

[52] M. Elyasi, M.A. Khalilzadeh, H. Karimi-Maleh, High sensitive voltammetric sensor based on Pt/CNTs nanocomposite modified ionic liquid carbon paste electrode for determination of Sudan I in food samples, Food chemistry, 141**(2013)** 4311-7.

[53] K. Kalcher, J.M. Kauffmann, J. Wang, I. Švancara, K. Vytřas, C. Neuhold, et al., Sensors based on carbon paste in electrochemical analysis: a review with particular emphasis on the period 1990–1993, Electroanalysis, 7**(1995)** 5-22.

[54] Q.A. Pankhurst, J. Connolly, S.K. Jones, J. Dobson, Applications of magnetic nanoparticles in biomedicine, Journal of physics D: Applied physics, 36**(2003)** R167.

[55] H. Teymourian, A. Salimi, S. Khezrian, Fe_3O_4 magnetic nanoparticles/reduced graphene oxide nanosheets as a novel electrochemical and bioeletrochemical sensing platform, Biosensors and Bioelectronics, 49**(2013)** 1-8.

[56] J. Willis, Determination of Lead and Other Heavy Metals in Urine by Atomic Absorption Spectroscopy, Analytical Chemistry, 34**(1962)** 614-7.

[57] V.L. Dressler, D. Pozebon, A.J. Curtius, Determination of heavy metals by inductively coupled plasma mass spectrometry after on-line separation and preconcentration, Spectrochimica Acta Part B: Atomic Spectroscopy, 53**(1998)** 1527-39.

[58] Y. Zhang, Y. Cheng, Y. Zhou, B. Li, W. Gu, X. Shi, et al., Electrochemical sensor for bisphenol A based on magnetic nanoparticles decorated reduced graphene oxide, Talanta, 107**(2013)** 211-8.

[59] W. Yantasee, K. Hongsirikarn, C.L. Warner, D. Choi, T. Sangvanich, M.B. Toloczko, et al., Direct detection of Pb in urine and Cd, Pb, Cu, and Ag in natural waters using electrochemical sensors immobilized with DMSA functionalized magnetic nanoparticles, Analyst, 133**(2008)** 348-55.

[60] A.K. Gupta, M. Gupta, Synthesis and surface engineering of iron oxide nanoparticles for biomedical applications, Biomaterials, 26**(2005)** 3995-4021.

[61] Y. Zhang, B. Chen, L. Zhang, J. Huang, F. Chen, Z. Yang, et al., Controlled assembly of Fe_3O_4 magnetic nanoparticles on graphene oxide, Nanoscale, 3**(2011)** 1446-50.

[62] S.K. Toor, P. Devi, B.K.S. Bansod, Electrochemical Detection of Trace Amount of Arsenic (III) at Glassy Carbon Electrode Modified with Au/Fe_3O_4 Nanocomposites, Aquatic Procedia, 4**(2015)** 1107-13.

[63] Z. Xu, Y. Hou, S. Sun, Magnetic core/shell Fe_3O_4/Au and Fe_3O_4/Au/Ag nanoparticles with tunable plasmonic properties, Journal of the American Chemical Society, 129**(2007)** 8698-9.

[64] M.R.H. Syed Kamrul Islam, Sensors and Low Power Signal Processing.

[65] N. Kumar, P. Sahatiya, P. Dubey, Fabrication of CNT based gas sensor using interdigitated gold electrodes, Procedia Materials Science, 6**(2014)** 1976-80.

[66] S. Kim, G. Yu, T. Kim, K. Shin, J. Yoon, Rapid bacterial detection with an interdigitated array electrode by electrochemical impedance spectroscopy, Electrochimica Acta, 82**(2012)** 126-31.

[67] H.F. Hawari, N.M. Samsudin, A.Y.M. Shakaff, S.A. Ghani, M.N. Ahmad, Y. Wahab, et al., Development of Interdigitated Electrode Molecular Imprinted Polymer Sensor for Monitoring Alpha Pinene Emissions from Mango Fruit, Procedia Engineering, 53**(2013)** 197-202.

[68] Y. Iwasaki, M. Morita, K. Atsugi, Electrochemical measurements with interdigitated array microelectrodes, Current separations, 14**(1995)** 2-8.

[69] A.E. Cohen, R.R. Kunz, Large-area interdigitated array microelectrodes for electrochemical sensing, Sensors and Actuators B: Chemical, 62**(2000)** 23-9.

[70] J. Li, Y. Lu, Q. Ye, M. Cinke, J. Han, M. Meyyappan, Carbon nanotube sensors for gas and organic vapor detection, Nano letters, 3**(2003)** 929-33.

[71] R. Ehret, W. Baumann, M. Brischwein, A. Schwinde, K. Stegbauer, B. Wolf, Monitoring of cellular behaviour by impedance measurements on interdigitated electrode structures, Biosensors and Bioelectronics, 12**(1997)** 29-41.

[72] K.V. Singh, A.M. Whited, Y. Ragineni, T.W. Barrett, J. King, R. Solanki, 3D nanogap interdigitated electrode array biosensors, Analytical and bioanalytical chemistry, 397**(2010)** 1493-502.

[73] W. Qu, J.-U. Meyer, A novel thick-film ceramic humidity sensor, Sensors and Actuators B: Chemical, 40**(1997)** 175-82.

[74] I. Gul, W. Ahmed, A. Maqsood, Electrical and magnetic characterization of nanocrystalline Ni–Zn ferrite synthesis by co-precipitation route, Journal of Magnetism and Magnetic Materials, 320**(2008)** 270-5.

[75] K. Maaz, S. Karim, A. Mumtaz, S. Hasanain, J. Liu, J. Duan, Synthesis and magnetic characterization of nickel ferrite nanoparticles prepared by co-precipitation route, Journal of Magnetism and Magnetic Materials, 321**(2009)** 1838-42.

[76] Z. Zi, Y. Sun, X. Zhu, Z. Yang, J. Dai, W. Song, Synthesis and magnetic properties of $CoFe_2O_4$ ferrite nanoparticles, Journal of Magnetism and Magnetic Materials, 321**(2009)** 1251-5.

[77] C. Peng, B. Chen, Y. Qin, S. Yang, C. Li, Y. Zuo, et al., Facile ultrasonic synthesis of CoO quantum dot/graphene nanosheet composites with high lithium storage capacity, ACS nano, 6**(2012)** 1074-81.

[78] W.D. Callister, D.G. Rethwisch, Materials science and engineering: an introduction: Wiley New York; **2007**.

[79] C.R. Brundle, C.A. Evans, S. Wilson, Encyclopedia of materials characterization: surfaces, interfaces, thin films: Gulf Professional Publishing; **1992**.

[80] E.N. KAUFMANN, Characterization of materials Hoboken, New Jersey: John Wiley & Sons, Inc., ; **2003**.

[81] N. Aristov, A. Habekost, Cyclic voltammetry-A versatile electrochemical method investigating electron transfer processes, World Journal of Chemical Education, 3**(2015)** 115-9.

[82] J.F. Rusling, S.L. Suib, Characterizing materials with cyclic voltammetry, Advanced Materials, 6**(1994)** 922-30.

[83] M. Culebras, C.M. Gómez, A. Cantarero, Review on polymers for thermoelectric applications, Materials, 7**(2014)** 6701-32.

[84] N.G. Tsierkezos, Cyclic voltammetric studies of ferrocene in nonaqueous solvents in the temperature range from 248.15 to 298.15 K, Journal of Solution Chemistry, 36**(2007)** 289-302.

[85] F. Zhao, R.C. Slade, J.R. Varcoe, Techniques for the study and development of microbial fuel cells: an electrochemical perspective, Chemical Society Reviews, 38**(2009)** 1926-39.

[86] G. Popkirov, R. Schindler, Validation of experimental data in electrochemical impedance spectroscopy, Electrochimica acta, 38**(1993)** 861-7.

[87] D. Zhu, W.J. Van Ooij, Structural characterization of bis-[triethoxysilylpropyl] tetrasulfide and bis-[trimethoxysilylpropyl] amine silanes by Fourier-transform infrared spectroscopy and electrochemical impedance spectroscopy, Journal of adhesion science and technology, 16**(2002)** 1235-60.

[88] E.P. Randviir, C.E. Banks, Electrochemical impedance spectroscopy: an overview of bioanalytical applications, Analytical Methods, 5**(2013)** 1098-115.

[89] A.M.A. Alsamuraee, H.I. Jaafer, Electrochemical impedance spectroscopic evaluation of corrosion protection properties of polyurethane/polyvinyl chloride blend coatings on steel Abdulkareem Mohammed Ali Alsamuraee1, Harith Ibraheem Jaafer2, Hani Aziz Ameen3 and Ahmed Qasim Abdullah4, **(2011)**.